INTERNATIONAL JOURNAL OF CIRCUIT THEORY AND APPLICATIONS
Int. J. Circ. Theor. Appl. 2018; **46**:184–220
Published online 30 November 2017 in Wiley Online Library (wileyonlinelibrary.com). DOI: 10.1002/cta.2430

SPECIAL ISSUE PAPER

Memristor-enhanced humanoid robot control system – Part II: Circuit theoretic model and performance analysis

D. Baumann[2], A. Ascoli[1,*,†], R. Tetzlaff[1], L.O. Chua[3] and M. Hild[4]

[1]*Institute of Circuits and Systems, Faculty of Electrical and Computer Engineering, Technische Universität Dresden, Dresden, Germany*
[2]*Autonomous Motion Department, Max Planck Institute for Intelligent Systems, Tübingen, Germany*
[3]*Department of Electrical Engineering and Computer Sciences, University of California Berkeley, Berkeley, CA, USA*
[4]*Fachbereich VII, Forschungslabor Neurorobotik, Beuth Hochschule für Technik Berlin, Berlin, Germany*

SUMMARY

Neuromorphic circuits shall be considered in electronics to perform complex computing tasks in a time-efficient and energy-efficient fashion and to adapt their problem-solving methodologies to changes in initial conditions and parameters. One of the key biological paradigms at the basis of their operation, allowing them to exhibit higher performance levels as compared with state-of-the-art electronic systems, is the mem-computing functionality, i.e. the capability to process and store data in the same physical location, which represents the core principle to overcome the time inefficiency of von Neumann machine architectures. With the advent of memristors, the interest in the exploitation of this principle to develop dynamic circuits for the implementation of innovative signal processing strategies has grown considerably. Here, we leverage the mem-computing capability inherent in these devices to propose an innovative control system for motion control in a humanoid robot. In the part I paper, we introduced the paradigm theoretic foundations. In this part II manuscript, we propose circuit-theoretic models for the new control system based upon an ideal and upon a physical memristor model and demonstrate through numerical simulations how it outperforms the old approach in terms of time-efficiency and energy-efficiency, maintaining a good degree of adaptability to changes in environmental conditions.

Received 15 August 2017; Revised 25 September 2017; Accepted 3 October 2017

KEY WORDS: memristor; circuit theory; nonlinear dynamics theory; control theory; adaptive circuits; robotics

1. INTRODUCTION

The control of a humanoid robot is typically based upon the selection of a certain strategy, the development of a model for its implementation, the coding of the mathematical description through a proper programming language and the final code execution through the use of suitable microcontrollers. In the humanoid robot Myon [1], a completely different control approach is employed. Each joint of Myon hosts the hardware realisation of a cognitive sensorimotor loop (CSL) [2] capable to implement various control strategies depending upon an attractor-based behaviour control learning scheme [3]. The supervised loop is an innovative bio-inspired artificial neural network leveraging solely on the inherently complex behaviour of a number of analog circuits, interacting crucially with a motor with combined sensor-actuator role to control the hosting joint independently from the rest of the robot's body. One of the strategies implemented in the state-of-the-art CSL hardware realisation within a joint of Myon, the so-called 'Go-Against-the-Force' (GAF) paradigm [4], induces the limb attached to the

*Correspondence to: A. Ascoli, Institute of Circuits and Systems, Faculty of Electrical and Computer Engineering, Technische Universität Dresden, Dresden, Germany.
†E-mail: alon.ascoli@tu-dresden.de

hosting joint to raise from a rest state up to a desired height and stabilises the target position thereafter. Despite being robust and stable [4], the GAF control paradigm has its own weaknesses when it comes to energy efficiency, speed and adaptability to changes in the external environment. These issues may be resolved through the introduction of a novel strategy revolving upon the memory, learning and computing capabilities of a non-volatile memristor [5–10]. The system-theoretic principles lying at the basis of the innovative control strategy, inspired to the Maximum Principle of Pontryagin [11] and named 'Kick-Fly-Catch' (KFC) paradigm, were laid down in the part I companion paper [12]. In this part II manuscript, we first propose a circuit-theoretic model for the new limb motion control system and then demonstrate through LTSpice simulations [13] how it outperforms the original approach in terms of movement speed and power consumption, maintaining a satisfactory level of adaptability to changes in the limb topology. As for the mathematical modelling of the core mem-computing element in the proposed control circuit, an ideal memristor [14] was first employed to demonstrate the validity of the theoretical findings reported in the part I paper. With the later adoption of the model of a physical nano-device [15] fabricated at Knowm, Inc. [16] to characterise the memristor device, because of the poor performance of real memristors as integrators, the circuitry implementing the proposed control strategy had to be modified so as to estimate the duration of a kick phase [12] by replacing the analog input-driven memristance programming circuit used for the ideal memristor with a pulse-based conductance modulation electronic system. The control circuit based on the physical memristor attained similar performance levels as the ideal memristor equivalent, except for a weaker adaptability to changes in the limb topology, because of the highly nonlinear dependence of the response of a memristor nano-device to a given aperiodic stimulus upon the initial condition. In view of the great deal of efforts devoted nowadays to reengineer memristor fabrication materials and processes so as to modulate the device electric properties to fit a particular application, this issue should be resolved in the future, when physical memristors with a more controlled dynamic behaviour shall be offered on the electronics market.

2. BRIEF REVIEW OF THE KICK-FLY-CATCH CONTROL STRATEGY

The block diagram of the motor-pendulum system under the proposed KFC control paradigm, whose theoretic foundations were laid in the part I companion paper [12], is shown in Figure 1(a). The voltage v_A at the armature node of the rotor stage is first set to the maximum possible control voltage $v_{ctrl,max}$ over a kick phase. This is enabled by a switch, here named $S_{kick\text{-}fly}$, which, clicked into its uppermost configuration, allows the transfer of the direct current (DC) 'kick' voltage $v_{ctrl,max}$, chosen as the positive supply level v_{B+} in the control circuit, to the armature node via an impedance converter. The final time of a kick phase, denoted here simply as $t_{f,k}$, is proportional to the output of a non-inverting integrator

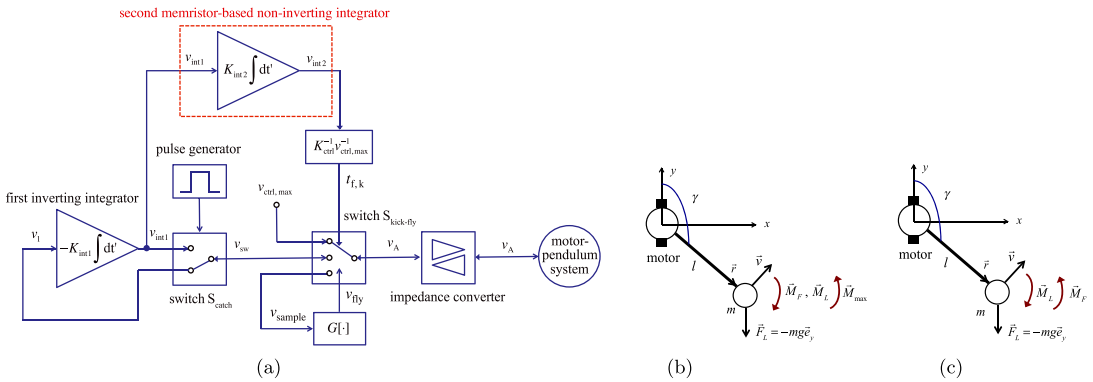

Figure 1. Block diagram of the proposed Kick-Fly-Catch cognitive sensorimotor loop strategy (a). The inverted pendulum over a typical kick phase (b) and fly phase (c) under the hypothesis $\gamma \in [0, \pi]$. $\vec{F}_L$ denotes the gravitation force ($g = 9.81$ m/s^2 is the gravitational acceleration). [Colour figure can be viewed at wileyonlinelibrary.com]

DOI: 10.1002/cta

at the end of the previous catch phase[‡] (see the companion part I paper [12] for details). For simplicity, an inverted pendulum system with rod length l and load mass m is adopted in our work to model the joint-limb topology of the humanoid robot Myon [1]. The pendulum angle γ is defined as the angle between the unit vector $\vec{e}_y$ and the vector $\vec{r}$ defining the position of the mass in the cartesian coordinate system. Figure 1(b) illustrates, under the hypothesis $\gamma \in [0, \pi]$[§], the torques acting on the load of mass m during a typical kick phase, i.e. one, $\vec{M}_L$, due to gravitation, one, $\vec{M}_F$, due to friction and one, the maximum possible motor torque $\vec{M}_{\max}$, due to the application of the maximum control voltage to the armature node. The 'kick' is properly fitted to the particular geometry of the pendulum and to the initial conditions of the dynamic system under control through an initialisation phase in which the old GAF paradigm is applied to the motor-pendulum system. The kick phase allows a fast lift of the pendulum from the stable rest state up to a position very close to the upright unstable state, ideally keeping on the same side of the x axis (refer to plot (b) in Figure 1). When the kick phase comes to an end, the switch $S_{\text{kick-fly}}$ is configured into its lowermost position, thus the pendulum is left free to move autonomously (see Figure 1(c) for a sketch of the torques in action on the load mass during a typical fly phase), while a nonlinear system with operator $G[\cdot]$ monitors the sign and modulus of the voltage v_{sample} at its input, coincident with the armature voltage v_{A}, in its turn identically equal to the electromotive force v_{ind} falling across the motor terminals (see Ascoli *et al.* [12] for details). When either v_{A} changes sign – here, the pendulum ascent has come to a halt before the target position, and its inevitable descent from the same side of the x axis (refer to plot (c) in Figure 1) has just commenced – or increases in modulus – here, the pendulum has just passed over the upright position and is about to descend from the other side of the x axis – the nonlinear memory block with operator $G[\cdot]$ outputs a positive voltage v_{fly}, triggering a new transition of the switch $S_{\text{kick-fly}}$, which is now set into its middle position, signalling the end of the fly phase. In the remaining time, the system operates in the catch phase. Similarly, as under GAF control, by means of a pulse generator a switch, here named S_{catch}, is alternatively clicked into its lower or upper position, allowing to sense the voltage at the armature node, here, tracking identically the motor electromotive force, which is coincidentally integrated with negative sign by the first integrator (the control system operates in sensing mode then), or to apply a DC voltage equal to the output of the first inverting integrator at the end of the previous sensing interval to the armature node, thus inducing a motor torque, which, acting on the pendulum mass, lifts it up winning over the opposing gravitation and friction torques (this is the driving mode control operation). In case of perturbations to initial conditions or modifications in the pendulum geometry, the kick phase duration, fitted to the nominal case, is no longer appropriate. This possible potential issue is addressed by the KFC control system, which throughout the catch phase, integrates the first integrator output voltage v_{int1} to update the estimate for the kick phase duration for a future application of the control strategy.

Remark 1

To accomplish the second integration task, the use of a memristor is crucial, because its innate mem-computing capability allows to process the integrand signal and to store the integration result v_{int2} from the end of the current catch phase till the beginning of a successive catch phase in a future run of the strategy or when the Myon is set into sleep mode. The signal integration itself could also be carried out by a capacitor, which, however, would not exhibit the same capability of a nonvolatile memristor to keep the information embedded in its state from the end of a catch phase to the beginning of a next one in a future application of the KFC strategy, or when the robot is turned off. In other words, the nonvolatile memory capability of memristors of a certain class is the key feature that naturally guides our proposal for a nonvolatile resistive memory cell-based control strategy for limb movement in Myon, as discussed in this two-part manuscript.

[‡]Note that the integrator with integration constant K_{int2} is inactive during the kick and fly phases, when its input voltage is grounded.

[§]Throughout this paper, we shall investigate the dynamics of the inverted pendulum under positive 'kick' stimuli for an initial pendulum angle equivalent to a small positive perturbation from the stable equilibrium in $\gamma = \pi$, leading to the rod ascent from the positive side of the x axis. Similar conclusions may be drawn under negative 'kick' stimuli for an initial pendulum angle equivalent to a small positive perturbation from the stable equilibrium in $\gamma = -\pi$, leading to the rod ascent from the negative side of the x axis.

DOI: 10.1002/cta

3. MEMRISTOR MODELS

In this section, we introduce the memristor models adopted later in the circuit-theoretic models of the novel KFC control strategy. Section 3.1 describes the ideal memristor emulator originally proposed in [14], while Section 3.2 reviews the generalised metastable switch (MSS) memristor model [15] of a real nano-device fabricated at Knowm, Inc. [16].

3.1. Ideal memristor emulator

The first memristor model chosen to test the novel strategy is the linear dopant drift mathematical description of the titanium dioxide (TiO_2) nano-device fabricated in 2008 at Hewlett Packard Labs [17]. Despite that it is an obsolete model, its use allows to gain a preliminary understanding of the mechanisms behind the application of the novel control strategy, in preparation for its implementation based upon the use of a real device, to be discussed later in the manuscript. The linear dopant drift model falls into the class of ideal generic current-controlled memristors according to the latest classification reported in [10]. It is well-known that every ideal generic memristor is equivalent to an ideal memristor. For this reason, the circuit implementation of the aforementioned model, described next and first introduced in [14], is referred to as ideal memristor emulator throughout this paper. The circuit presented in [14] has two variants, known as incremental and decremental memristor emulators, allowing the memristance to increase and decrease under a positive input current, respectively (the opposite change in memristance would occur under a negative input current, because the model captures bipolar memristive dynamics [18]). A simplified schematics for the decremental configuration, used in this research work and properly matching the behaviour of the Hewlett Packard memristor, is shown in Figure 2.

The voltage v_m across the memristor is defined as the circuit input voltage v_in and can be calculated via

$$v_\mathrm{m} = R_\mathrm{s} i_\mathrm{m} - v_\mathrm{x}, \tag{1}$$

where the current i_m through the emulator is modelled by the circuit input current i_in. The voltage v_x at the output of the multiplier is obtained by scaling the product between the voltages across capacitor C_T and resistor R_T, i.e.

$$v_\mathrm{x} = k_\mathrm{conv,8} \frac{q_\mathrm{T}}{C_\mathrm{T}} R_\mathrm{T} i_\mathrm{m}, \tag{2}$$

with q_T denoting the capacitor charge, and $k_\mathrm{conv,8}$ representing a unitary constant with units V^{-1}. Now, inserting Equation (2) into Equation (1), and noting that q_T, obtained by integrating i_in over time, mimics the memristor charge q_m, we obtain:

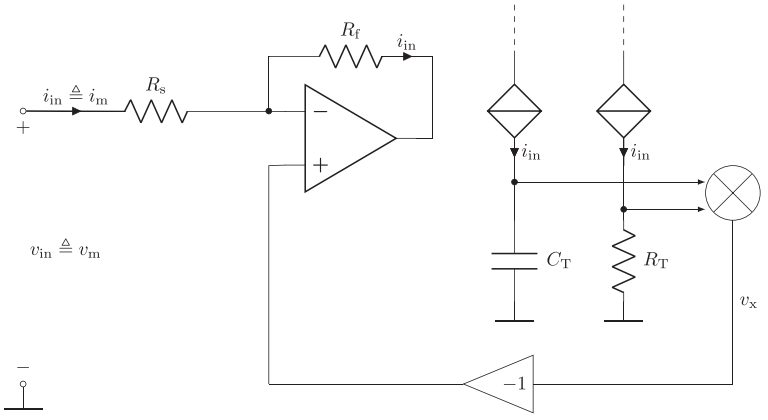

Figure 2. Simplified schematics for the decremental memristor emulator from Kim *et al.* [14].

DOI: 10.1002/cta

$$v_{\mathrm{m}} = \left(R_{\mathrm{s}} - k_{\mathrm{conv},8} \frac{q_{\mathrm{m}}}{C_{\mathrm{T}}} R_{\mathrm{T}} \right) i_{\mathrm{m}}. \tag{3}$$

Thus, the memristance of the current-controlled ideal memristor emulator, equivalent to the circuit input resistance, is expressed at any time t by

$$R\left(q_{\mathrm{m}}(t)\right) = \frac{v_{\mathrm{m}}(t)}{i_{\mathrm{m}}(t)} = R_{\mathrm{s}} - k_{\mathrm{conv},8} \frac{R_{\mathrm{T}}}{C_{\mathrm{T}}} q_{\mathrm{m}}(t), \tag{4}$$

where the charge $q_m(t)$ may be derived via the following equation

$$q_{\mathrm{m}}(t) = q_{\mathrm{m}}(t_{\mathrm{i}}) + \int_{t_{\mathrm{i}}}^{t} i_{\mathrm{m}}(t')\, \mathrm{d}t', \tag{5}$$

with t_{i} as prescribed initial time for the circuit analysis. Thus, the memristance of the emulator decreases (increases) proportionally to the time integral of a positive (negative)-signed current i_m flowing through it. This explains the decremental attribute conferred to this circuit configuration. Finally, the mathematical description of the ideal memristor emulator, including the state-dependent Ohm's law, resulting from Equation (4), and the state equation consisting of the differential relation between memristor charge and memristor current [10], is expressed by

$$\frac{dq_{\mathrm{m}}}{dt} = i_{\mathrm{m}}, \tag{6}$$

$$v_{\mathrm{m}} = R\left(q_{\mathrm{m}}\right) \cdot i_{\mathrm{m}}, \tag{7}$$

where the expression for the memristance $R\left(q_{\mathrm{m}}\right)$ is given in Equation (4).

In the linear dopant drift model of the TiO_2 memristor, the state variable is defined as the length $w \in [0, D]$ of the device conductive layer (the full longitudinal extension of the nanostructure is D). The differential algebraic equation (DAE) set, composed of the state equation and of the state-dependent Ohm law, is expressed by

$$\frac{dw}{dt} = \frac{\mu \cdot R_{\mathrm{on}}}{D} \cdot i_{\mathrm{m}}. \tag{8}$$

$$v_{\mathrm{m}} = R(w) \cdot i_{\mathrm{m}}, \tag{9}$$

where μ represents the ion mobility in the TiO_2 nano-device, whose resistance, assuming values within the set $[R_{\mathrm{on}}, R_{\mathrm{off}}]$ is defined as

$$R(w) = R_{\mathrm{on}} \cdot \frac{w}{D} + R_{\mathrm{off}} \cdot \left(1 - \frac{w}{D}\right), \tag{10}$$

Now, integrating the state Equation (8), at any time t, the length w of the conductive layer of the memristor is defined as a function of the charge q_{m} flowing through it by the following analytical formula:

$$w(t) = \frac{\mu R_{\mathrm{on}}}{D} q_{\mathrm{m}}(t), \tag{11}$$

where $q_{\mathrm{m}}(t)$ is expressed by Equation (5).

Replacing the formula in Equation (11) into Equation (10), at any time t, the expression for the memristance of the TiO_2 device in terms of the charge flowing it may be cast as

$$R(q_{\mathrm{m}}(t)) = R_{\mathrm{off}} - \mu \frac{R_{on} R_{off}}{D^2} q_{\mathrm{m}}(t), \tag{12}$$

where we assumed that the device memristance in the off state (when $w = 0$) is much larger than the device memristance in the on state (when $w = D$), i.e. that the hypothesis $R_{\mathrm{off}} >> R_{\mathrm{on}}$ applies.

DOI: 10.1002/cta

It is instructive to note that the emulator resistance expressed by Equation (4) is equivalent to the memristance of the TiO_2 memristor, as predicted by the linear dopant drift model [17] and given in Equation (12), provided the following two conditions are satisfied as follows:

$$R_{\mathrm{s}} = R_{\mathrm{off}}, \tag{13}$$

$$k_{\mathrm{conv},8}\frac{R_{\mathrm{T}}}{C_{\mathrm{T}}} = \mu\frac{R_{on}R_{off}}{D^2}. \tag{14}$$

We wish to point out that the reason behind our choice to report all calculations in this section is motivated by our frequent reading of scientific contributions where the initial conditions are not taken into account in the integration of memristor state equations. Because the initial condition may play an important role in the dynamics of a memristor [19], its inclusion in the analysis of the device electrical properties is necessary.

3.2. Generalised Metastable Switch memristor model

The generalised MSS model [15] is a mathematical description capturing the dynamics of a wide range of memristor devices, including the resistance switching memory [6] manufactured by Knowm, Inc.[16]. According to this model, the current i_{m} through the memristor can be calculated as the sum of a memory-dependent current component i_{mss} and of a Schottky diode current component i_{s}, leading to

$$i_{\mathrm{m}} = \phi \cdot i_{\mathrm{mss}} + (1-\phi)\cdot i_{\mathrm{s}}, \tag{15}$$

where the constant $\phi \in [0,1]$ determines which of the two components has the most significant impact on the device dynamics. Now, letting v_{m} denote the voltage across the memristor, the Schottky diode current component, delivered by two Schottky diodes in antiparallel, may be described by

$$i_{\mathrm{s}} = \alpha_{\mathrm{f}}\exp\left(\beta_{\mathrm{f}}v_{\mathrm{m}}\right) - \alpha_{\mathrm{r}}\exp\left(-\beta_{\mathrm{r}}v_{\mathrm{m}}\right), \tag{16}$$

where α_{f} (α_{r}) and β_{f} (β_{r}) are non-negative parameters scaling amplitude and argument of the exponential current flowing through the forward (reverse)-biased diode, respectively. The memory-dependent current component is flowing through a collection of N_{tot} conducting channels running in parallel to the two Schottky diodes. Every channel is treated as a MSS, which at any given time operates in one of two possible states, referred to as 1 and 2 and which may switch from one of them to the other as time goes forward by one step Δt. The probability $P_{2\to1}$ that a MSS operating in state 2 at a given time instant will operate in state 1 at the following time instant is given by

$$P_{2\to1} = \alpha\cdot\Gamma\left(v_{\mathrm{m}}, V_{\mathrm{m},1}\right), \tag{17}$$

where the function $\Gamma(\cdot,\cdot)$ has the following closed-form expression:

$$\Gamma\left(v_{\mathrm{m}}, V_{\mathrm{m},1}\right) = \frac{1}{1+\exp\left(\frac{v_{\mathrm{m}}-V_{\mathrm{m},1}}{V_{\mathrm{T}}}\right)}. \tag{18}$$

Here, $V_{\mathrm{T}} = KT/q$ represents the thermal voltage ($K = 1.38\cdot10^{-23}\mathrm{J\cdot K^{-1}}$ is the Boltzmann constant, while $q = 1.6\cdot10^{-19}\mathrm{C}$ stands for the elementary electronic charge), approximately equal to 26mV at an ambient temperature T of 300K, α is the ratio between the time step Δt and the device characteristic time scale τ_{c}, and $V_{\mathrm{m},1}$ is the threshold voltage for a switch transition from state 2 to state 1. Now, the probability $P_{1\to2}$ that a MSS undergoes the complementary state transition from one instant to the following one is expressed as

$$P_{1\to2} = \alpha\left(1-\Gamma\left(v_{\mathrm{m}}, -V_{\mathrm{m},2}\right)\right), \tag{19}$$

where $V_{\mathrm{m},2}$ denotes the threshold voltage for a switch transition from state 1 to state 2.

DOI: 10.1002/cta

At any time, the following equality applies

$$N_{\text{tot}} = N_1 + N_2, \tag{20}$$

where N_1 and N_2 represent the number of MSSs in state 1 and 2, respectively. The population N_2 of MSS in state 2 may be interpreted as memristor state here (at any given time, N_1 may be easily extracted from the knowledge of N_2 via Equation (20)).

Each state has an intrinsic electrical conductance, namely G_1 and G_2 for state 1 and 2, respectively. It is further assumed that $G_2 > G_1$. At any given time, the total memory conductance $G(N_2)$ of the collection of N_{tot} parallel channels is simply the sum of the conductances of all the switches:

$$G\left(N_2\right) = \left(N_{\text{tot}} - N_2\right) G_1 + N_2 G_2, \tag{21}$$

Of course the total memory-resistance $R(N_2)$ of the collection of N_{tot} parallel channels is defined as the inverse of the memory-conductance expressed by Equation (21), i.e.

$$R\left(N_2\right) = \left(\left(N_{\text{tot}} - N_2\right) G_1 + N_2 G_2\right)^{-1}. \tag{22}$$

For each of the two states, the probability that from one instant to the following one x MSSs out of a population of n elements will undergo a transition to the other state that is governed by a binomial distribution, which, for large values of n, may be approximated by a normal distribution, i.e.

$$\mathcal{N}_{\mu,\sigma}(x) = \frac{1}{\sqrt{2\pi\sigma^2}} \cdot \exp\left(-\frac{(x-\mu)^2}{2\sigma^2}\right), \tag{23}$$

with the expected value $\mu = n \cdot p$ and the variance $\sigma^2 = n \cdot p\,(1-p)$, where p denotes the probability of state transition for a single switch during the given time step (depending on the state under consideration n and p correspondingly assume values in (N_2, N_1) and in $(P_{2\to1}, P_{1\to2})$).

During the time step from one instant to the following one, for each state, the relevant normal distribution is sampled to select randomly the number x of MSSs undergoing a transition to the other state. Denoting with $\Delta N_{2\to1}$, the random number of conducting channels switching from states 2 to 1, and with $\Delta N_{1\to2}$, the random number of MSSs undergoing the complementary transition, the change ΔG in the total memductance of the collection of N_{tot} channels can be calculated through

$$\Delta G\left(\Delta N_{2\to1}, \Delta N_{1\to2}\right) = \left(\Delta N_{1\to2} - \Delta N_{2\to1}\right)\left(G_2 - G_1\right). \tag{24}$$

Finally, the memory-dependent component i_{mss} in the expression for the device current i_{m} is obtained from

$$i_{\text{mss}} = \left(G(N_2) + \Delta G\left(\Delta N_{2\to1}, \Delta N_{1\to2}\right)\right) \cdot v_{\text{m}}. \tag{25}$$

4. IDEAL MEMRISTOR-BASED CIRCUIT-THEORETIC MODEL OF THE KICK-FLY-CATCH CONTROL PARADIGM

In this section, we adopt the ideal memristor emulator of Section 3.1 to propose a circuit-theoretic model of the novel KFC control strategy.

The electrical part of the rotor stage under KFC control is modelled by the circuits in plots (a), (b) and (c) of Figure 3. This circuitry is a modified version of the corresponding electronic system under GAF control, which is shown in Figure 5 of the part I paper [12]. With reference to Figure 3, the plot (a) shows the voltage source v_{timer} dictating the alternation of sense and drive phases and controlling the voltage-controlled sources in the circuits of plots (b) and (c). The plot (b) illustrates the armature circuit with the current-controlled source modelling the motor electromotive force v_{ind}, the current i_{A} standing for the armature current and the node A denoting the armature node, playing a crucial role in both the GAF and the KFC control strategies. The plot (c) depicts the circuit modelling the inverting integration of the armature voltage over a sense phase. At the start of a new KFC strategy run, i.e. at the

DOI: 10.1002/cta

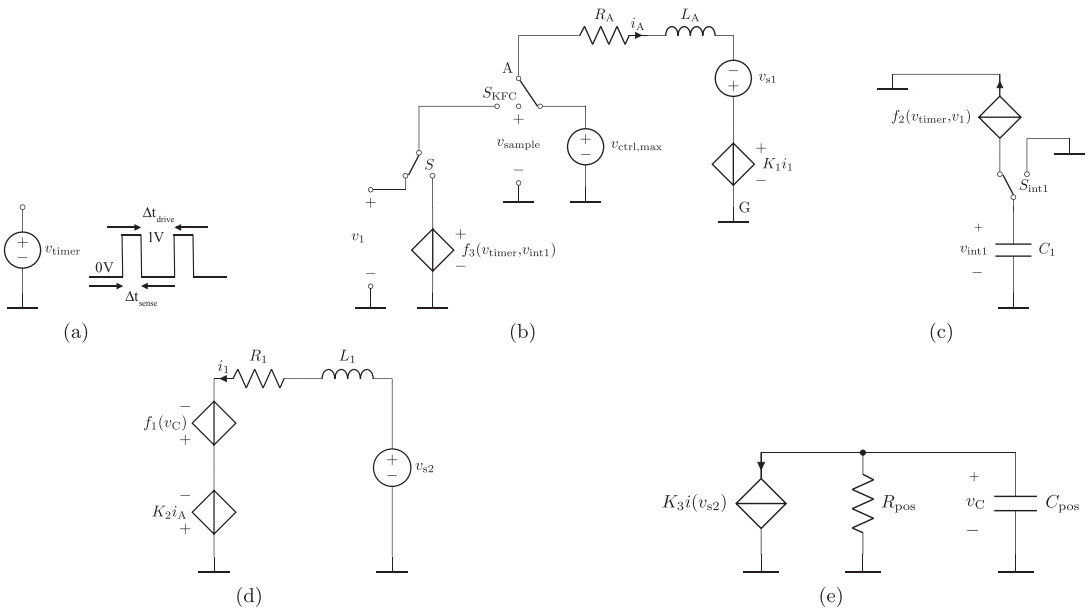

Figure 3. Circuit theoretic implementation of the electromechanical model of the motor-pendulum system under Kick-Fly-Catch cognitive sensorimotor loop control. (a) Voltage source v_{timer} generating a square waveform – in the inset – dictating the cyclic alternation between sensing and driving operations over a catch phase in the circuits of plots (b) and (c) by means of the control of the switch S and of the two voltage-controlled sources $f_2(\cdot,\cdot)$ and $f_3(\cdot,\cdot)$ (see the part I paper [12] for details on their mathematical expressions). (b) Electrical part of the rotor stage endowed with a two switch-based control circuit for the implementation of the three phases of the Kick-Fly-Catch paradigm. (c) Circuit implementing the inverting integration of the armature voltage in the sense mode of a catch phase. During a kick phase, the maximum possible control voltage $v_{\text{ctrl,max}} = v_{\text{B+}}$ is applied to the armature node A in plot (b), while the first integrator output voltage v_{int1} in plot (c) is forced to 0 V. The time at which the kick phase comes to an end is determined by the circuits in Figures 4(b)–(e) on the basis of a memristor-based non-inverting integration of the voltage v_{int1} carried out in the preceding catch phase (refer to the circuit in plot (a) of Figure 4). During a fly phase, the armature node voltage in plot (b) is inserted to the input v_{sample} of a monitoring circuit – refer to Figure 5 – to detect the time at which the catch phase should commence. Over the catch phase, the 0 V clamp applied to the first integrator output is released. In the sense mode, the armature node A in plot (b) is coupled to the input of the first inverting integrator at voltage v_1, while in drive mode v_{A} is constrained to follow the direct current voltage v_{int1} at the end of the preceding sense mode phase. As mentioned earlier, throughout the catch phase, the first integrator output voltage v_{int1} is further integrated with positive integration constant through the use of a memristor (see the circuit of Figure 4(a)). The second integration result is then used (via the circuits in Figures 4(b)–(e)) during a subsequent kick phase to improve the estimate of the time at which the fly phase should commence. (d) Circuit modelling the mechanical part of the rotor stage and the loaded rod attached to the motor. (e) Circuit calculating the pendulum angle.

beginning of a novel kick phase, the switch S_{int1} is clicked into its right position, thus forcing to zero the initial condition for the first integrator output voltage v_{int1}. As mentioned in Section 2, the inverting integrator circuit in plot (c) is inactive during kick and fly phases. With reference to plot (b), at the start of a kick phase, the switch S_{KFC} is clicked into the rightmost configuration, enforcing the maximum possible control voltage to the armature node. Meanwhile, a new circuit (to be introduced later, see Figure 4(b)–(e)) detects the time instant at which the kick phase leaves the 'stage' to the fly phase (on the basis of the non-inverting integration carried out in the preceding catch phase by yet another circuit to be presented shortly, see Figure 4(a)). When this occurs, the switch S_{KFC} is configured to the middle position. At that point, the voltage v_{sample} at the input to the memory block with nonlinear operator $G[\cdot]$, whose circuit implementation will be presented later (see Figure 5), coincides with the armature voltage v_{A}, allowing the monitoring of the sign and modulus of the pendulum angular velocity ω (in this phase, the armature voltage coincides with the electromotive force $v_{\text{ind}} = c\varphi\omega$, where c and φ, respectively, denote the positive dimensionless motor constant and the unvarying flux generated by the stator stage). When the fly phase comes to an end (see Section 2 for details), the switch S_{KFC} in plot (b)

DOI: 10.1002/cta

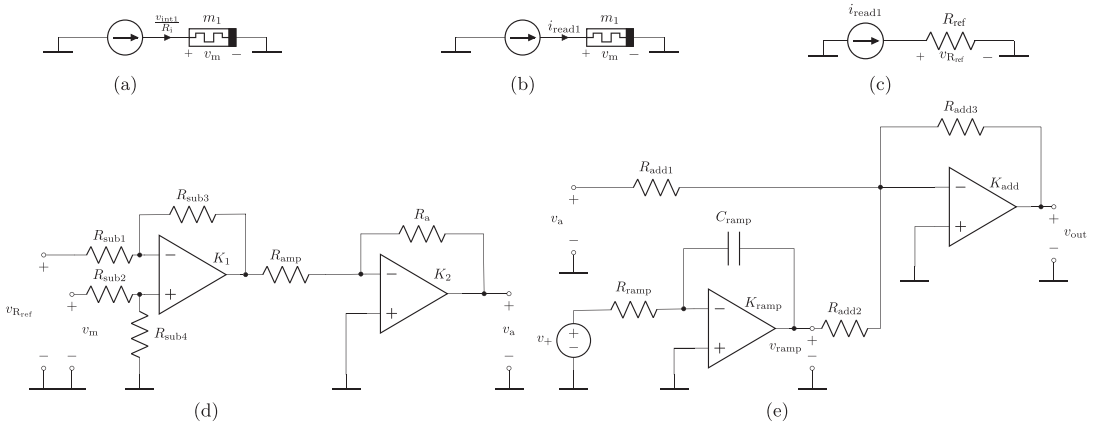

Figure 4. Part of the circuit-theoretic model of the KFC control paradigm leveraging the mem-computing capability of the ideal memristor emulator of Figure 2. (a) Circuit active throughout the jth catch phase and updating the memristance $R(q_{\mathrm{m}})$ of the memristor m_1 by letting a current proportional to the first inverting integrator output voltage v_{int1} flow through it. (b), (c) Reading circuits for the memristance $R(q_{\mathrm{m}})$ and for the reference resistance R_{ref}, respectively. The reading is performed throughout the $(j+1)$th kick phase. (d) Circuit enabling the availability of a scaled version of the constant voltage $v_{\mathrm{int2}}(t_{\mathrm{f,c}}^{(j)})$ at the output node at voltage v_{a} throughout the $(j+1)$th kick phase (the scaling factor is $\rho = v_{+}/v_{\mathrm{ctrl,max}}$). (e) Circuit allowing the determination of the final time $t_{\mathrm{f,k}}^{(j+1)}$ of the $(j+1)$th kick phase.

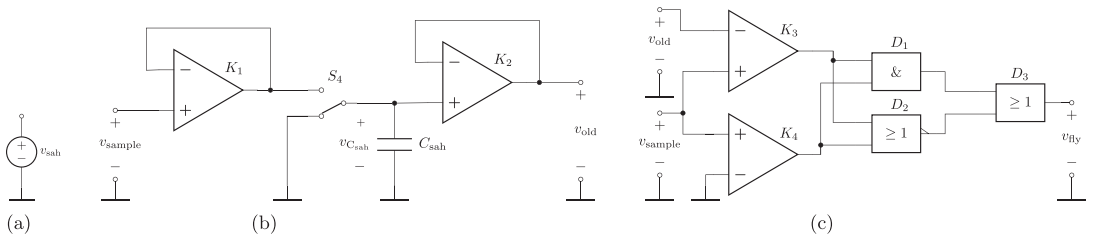

Figure 5. Circuit allowing the determination of the duration of the $(j+1)$th fly phase. (a) Pulse voltage generator controlling the timing of the sample-and-hold circuit. (b) Sample-and-hold circuit used in the fly phase to store in the voltage variable v_{old} the last value for the input signal v_{sample}, which in our case study – see the block diagram of the overall system under Kick-Fly-Catch cognitive sensorimotor loop control in Figure 1(a) – coincides here with the armature node voltage v_{A}. (c) Hybrid analog-digital circuit for the detection of the time at which $v_{\mathrm{sample}} \equiv v_{\mathrm{A}}$ increases in modulus or changes polarity. The saturation levels of the operational amplifiers, equal to the supply voltages used in the circuit implementation of the Kick-Fly-Catch paradigm, are $\pm 9\,V$. Regarding the logic circuitry, D_1, D_2 and D_3 are an AND, a NOR and an OR gate, respectively. A positive value for v_{fly} would lead to the click of the switch $S_{\text{kick-fly}}$ in Figure 1(a) into its centre configuration, and the $(j+1)$th catch phase would be initiated with a sense phase.

assumes the left-most configuration, the switch S_{int1} in plot (c) connected the controlled current source to the capacitor and the system operates in the same fashion as under GAF control (cf. Figure 5 in Ascoli *et al.* [12]). Cyclically, as clocked by the timer v_{timer} from plot (a), the switch S in plot (b) either couples the armature node to the input of the inverting integrator at voltage v_1 during a sense phase, when the controlled current source $f_2(v_{\mathrm{timer}}, v_1)$ in plot (c) extracts a current proportional to v_1 from the integrating capacitor or applies a DC voltage equal to the output of the inverting integrator at the end of the previous sense phase to the armature node itself through the voltage-controlled voltage source $f_3(v_{\mathrm{timer}}, v_{\mathrm{int1}})$ (in this phase, no current is sourced by the controlled current source in plot (c)). Over a catch phase, as mentioned earlier, the first integrator output voltage v_{int1} is integrated with positive sign. This operation, accomplished through the use of a memristor, as described shortly (refer to plot (a) in Figure 4), shall allow in the following kick phase to determine a better estimate for the beginning of the fly phase. The mechanical part of the rotor stage is modelled the same way as in the circuit-theoretic model of the GAF CSL-controlled system discussed in the part I paper [12] (see Figures 4

DOI: 10.1002/cta

(b) and (c) therein). For the sake of completeness, the circuitry is shown again in plots (c) and (d) of Figure 3. The circuit in the first plot implements Newton's Law for rotatory motion. Here, the action of friction, gravitation and motor torques on the pendulum load mass are, respectively, accounted for by the resistance, by the voltage-controlled voltage source and by the current-controlled voltage source, the pendulum angular velocity is captured by the current i_1, whereas with the moment of inertia of the inverted pendulum is modelled by the inductance L_1. The circuit in the second plot realises the integral relation allowing the determination of the pendulum angle γ from its angular velocity ω. Here, the voltage across the capacitor models the pendulum angle. With regard to the complete circuitry in Figure 3, the definition of those symbols and function expressions, which were not given above, may be found in the companion part I paper [12]. The values for all the parameters in the circuits of this figure are reported in Table I in the part I paper [12], where the nominal values for the mass m and the length l of the rod load modelling a robot limb, accounted for through the use of the voltage-controlled voltage-source $f_1(v_C)$ in plot (d), are set to 10 g and 10 cm, respectively.

Using a voltage-controlled current source, a current proportional to the first inverting integrator output voltage v_{int1} shown in Figure 1(a) – the proportionality factor is indicated as R_i^{-1} with units S – is let flow through the memristor during a catch phase, i.e.

$$i_m(t) = \frac{v_{int1}(t)}{R_i} \tag{26}$$

as shown in Figure 4(a). The charge through the memristor emulator at the end of the catch phase for the jth iteration of the KFC strategy application ($j \in \mathbb{N} = \{1, 2, 3, \dots\}$), assumed to span the time interval $[t_{0,c}^{(j)}, t_{f,c}^{(j)}]$, is expressed by

$$\begin{aligned} q_m(t_{f,c}^{(j)}) &= q_m(t_{0,c}^{(j)}) + \int_{t_{0,c}^{(j)}}^{t_{f,c}^{(j)}} i_m(t')dt' \\ &= q_m(t_{0,c}^{(j)}) + \frac{1}{R_i}\int_{t_{0,c}^{(j)}}^{t_{f,c}^{(j)}} v_{int1}(t')dt' \end{aligned} \tag{27}$$

where the initial condition $q_m(t_{0,c}^{(j)})$ crucially depends upon the device history, i.e.

$$q_m(t_{0,c}^{(j)}) = q_m(t_{0,g}^{(0)}) + \frac{1}{R_i}\int_{t_{0,g}^{(0)}}^{t_{0,c}^{(j)}} v_{int1}(t')dt', \tag{28}$$

with $t_{0,g}^{(0)}$ denoting the initial time in the application of the old GAF strategy, also named initialisation phase, spanning the time interval $[t_{0,g}^{(0)}, t_{f,g}^{(0)}]$ [12] (a fictitious null value is attributed to the strategy run count variable j in this preliminary phase, whose initial time is defined as $t_i^{(0)} \triangleq t_{0,g}^{(0)}$ and set to 0 s).

Plots (b) and (c) in Figure 4, respectively, show the memristance $R(q_m)$ and a reference resistance R_{ref} reading circuits used throughout the following $(j+1)$th kick phase[¶], going on throughout the time interval $[t_{0,k}^{(j+1)}, t_{f,k}^{(j+1)})$, as discussed in the part I paper [12]. With reference to Figure 4, the two reading

Table I. Parameters of the ideal memristor emulator of Figure 2.

Parameter	Value	Parameter	Value
R_s	16 kΩ	R_f	16 kΩ
R_T	4 kΩ	C_T	100 μF

[¶]In principle, the memristance reading operation could be carried out just once at the end of the jth catch phase. However, in order to simplify the circuit implementation, such measurement is here performed throughout the kick phase, relying upon the fairly non-disruptive nature of the reading process guaranteed by a suitable choice of the sensing current signal i_{read1} (see later for details on such choice).

DOI: 10.1002/cta

circuits in plots (b) and (c) are used in the circuit of plot (d) to read throughout the $(j+1)$th kick phase a constant voltage signal v_{a} (note that this is not the voltage at the armature node A, which is indicated as v_{A} instead, as established in the part I paper [12]) proportional to the voltage $v_{\mathrm{int2}}(t_{\mathrm{f,c}}^{(j)})$ at the output of the second non-inverting integrator shown in Figure 1(a) at the end of the j^{th} catch phase (assuming an ideal memristance reading process, this voltage maintains unaltered over the course of the $(j+1)$th kick phase). Using unitary-gain voltage-controlled voltage sources, the voltages across the memristor $v_{\mathrm{m}}(t_{\mathrm{f,c}}^{(j)}) = R(q_{\mathrm{m}}(t_{\mathrm{f,c}}^{(j)}))i_{\mathrm{read1}}$ and the reference resistor $v_{R_{\mathrm{ref}}} = R_{\mathrm{ref}} i_{\mathrm{read1}}$ are inserted to the inputs of the circuit in plot (d), where they are subtracted from the first operational amplifier (op amp) stage and then amplified by the following inverting amplifier, resulting in this expression for the output voltage v_{a}:

$$\begin{aligned} v_{\mathrm{a}} &= -\frac{R_{\mathrm{a}}}{R_{\mathrm{amp}}}\left(-\frac{R_{\mathrm{sub3}}}{R_{\mathrm{sub1}}}v_{R_{\mathrm{ref}}} + \frac{R_{\mathrm{sub4}}}{R_{\mathrm{sub2}}+R_{\mathrm{sub4}}}\frac{R_{\mathrm{sub1}}+R_{\mathrm{sub3}}}{R_{\mathrm{sub1}}}v_{\mathrm{m}}(t_{\mathrm{f,c}}^{(j)})\right) \\ &= -\frac{R_{\mathrm{a}}}{R_{\mathrm{amp}}}\left(-\frac{R_{\mathrm{sub3}}}{R_{\mathrm{sub1}}}R_{\mathrm{ref}} + \frac{R_{\mathrm{sub4}}}{R_{\mathrm{sub2}}+R_{\mathrm{sub4}}}\frac{R_{\mathrm{sub1}}+R_{\mathrm{sub3}}}{R_{\mathrm{sub1}}}R(q_{\mathrm{m}}(t_{\mathrm{f,c}}^{(j)}))\right) i_{\mathrm{read1}}. \end{aligned} \tag{29}$$

Letting $R_{\mathrm{sub1}} = R_{\mathrm{sub2}} = R_{\mathrm{sub3}} = R_{\mathrm{sub4}}$ and $R_{\mathrm{ref}} = R_{\mathrm{s}}$ (R_{s} appears in the schematics of the memristor emulator of Figure 2), and inserting Equation 4 into Equation 29, the analytical formula for the DC voltage v_{a} at the output of the circuit of Figure 4(d) throughout the $(j+1)$th kick phase may be recast as

$$v_{\mathrm{a}} = \frac{R_{\mathrm{a}}}{R_{\mathrm{amp}}}k_{\mathrm{conv,8}}\frac{R_{\mathrm{T}}}{C_{\mathrm{T}}}q_{\mathrm{m}}(t_{\mathrm{f,c}}^{(j)})i_{\mathrm{read1}} \tag{30}$$

where, as stated earlier, $k_{\mathrm{conv,8}}$ represents a unitary constant with units V^{-1}. Using Equations 27 and 28 into Equation 30, and letting

$$R_{\mathrm{a}} = C_{\mathrm{T}}R_{\mathrm{amp}}R_i k_{\mathrm{conv,9}} / \left(R_{\mathrm{T}} i_{\mathrm{read1}} v_{\mathrm{ctrl,max}}\right), \tag{31}$$

where $k_{\mathrm{conv,9}}$ is a factor with units $\mathrm{V}^2\mathrm{s}^{-1}$, and the constant voltage v_{a} may be rewritten as

$$\begin{aligned} v_{\mathrm{a}} &= \frac{k_{\mathrm{conv,8}}k_{\mathrm{conv,9}}}{v_{\mathrm{ctrl,max}}}\left(\int_{t_{0,\mathrm{g}}^{(0)}}^{t_{0,\mathrm{c}}^{(j)}} v_{\mathrm{int1}}(t')dt' + \int_{t_{0,\mathrm{c}}^{(j)}}^{t_{\mathrm{f,c}}^{(j)}} v_{\mathrm{int1}}(t')dt'\right) \\ &= \rho\, K_{\mathrm{int,2}}\left(\int_{t_{0,\mathrm{g}}^{(0)}}^{t_{0,\mathrm{c}}^{(j)}} v_{\mathrm{int1}}(t')dt' + \int_{t_{0,\mathrm{c}}^{(j)}}^{t_{\mathrm{f,c}}^{(j)}} v_{\mathrm{int1}}(t')dt'\right), \end{aligned} \tag{32}$$

where we defined K_{int2} as $K_{\mathrm{int2}} = k_{\mathrm{conv,8}}k_{\mathrm{conv,9}}/v_{+}$, with $v_{+} = 1\,\mathrm{V}$ and ρ as $\rho = v_{+}/v_{\mathrm{ctrl,max}}$ (note that K_{int2} has units s^{-1}, as expected). With reference to Figure 1(a), the second integrator output voltage at the end of the jth catch phase is expressed as

$$v_{\mathrm{int2}}(t_{\mathrm{f,c}}^{(j)}) = v_{\mathrm{int2}}(t_{0,\mathrm{g}}^{(0)}) + K_{\mathrm{int2}}\int_{t_{0,\mathrm{g}}^{(0)}}^{t_{0,\mathrm{c}}^{(j)}} v_{\mathrm{int1}}(t')dt' + K_{\mathrm{int2}}\int_{t_{0,\mathrm{c}}^{(j)}}^{t_{\mathrm{f,c}}^{(j)}} v_{\mathrm{int1}}(t')dt', \tag{33}$$

which may also be obtained by inserting Equation 30 into Equation 29 from the part I paper [12]. Noting that $v_{\mathrm{int2}}(t_{0,\mathrm{g}}^{(0)}) = 0\,\mathrm{V}$, using Equation 33, Equation 32 may be finally cast as

$$v_{\mathrm{a}} = \rho\, v_{\mathrm{int2}}(t_{\mathrm{f,c}}^{(j)}), \tag{34}$$

Thus, throughout the $(j+1)$th kick phase, the DC voltage v_{a} gives a scaled version of the output of the second non-inverting integrator shown in Figure 1(a) at the end of the jth catch phase.

Let us now explain how the $(j+1)$th kick phase is terminated, leaving the stage to the $(j+1)$th fly phase, active for the time interval $[t_{0,\mathrm{f}}^{(j+1)}, t_{\mathrm{f,f}}^{(j+1)})$ [12]. With reference to Figure 4, the circuit in plot (e), which operates throughout the $(j+1)$th kick phase, allows the estimation of the time instant $t_{0,\mathrm{f}}^{(j+1)} \equiv t_{\mathrm{f,k}}^{(j+1)}$ at which the $(j+1)$th fly phase should commence, on the basis of the calculation of the second non-inverting integrator output voltage $v_{\mathrm{int2}}(t_{\mathrm{f,c}}^{(j)})$ at the end of the jth catch phase, which is available at the

DOI: 10.1002/cta

output of the circuit of plot (d) throughout the $(j+1)$th kick phase. The inputs to the circuit in plot (e) are constant voltages v_{a}, expressed by Equation (34), and v_{+}, which, as defined earlier, is a scaled down version of the maximum operating voltage $v_{\mathrm{ctrl,max}}$ of the control circuit, i.e. $v_{+} = \rho v_{\mathrm{ctrl,max}}$. An op amp-based circuit integrates v_{+}, providing at its output the following ramp voltage:

$$\begin{aligned} v_{\mathrm{ramp}}(t) &= v_{\mathrm{ramp}}(t_{0,\mathrm{k}}^{(j+1)}) - \frac{1}{R_{\mathrm{ramp}}C_{\mathrm{ramp}}}\int_{t=t_{0,\mathrm{k}}^{(j+1)}}^{t} v_{+}dt \\ &= -\frac{1}{R_{\mathrm{ramp}}C_{\mathrm{ramp}}}v_{+}t, \end{aligned} \tag{35}$$

where $t_{0,\mathrm{k}}^{(j+1)} = 0\,\mathrm{s}$ (as described in Ascoli *et al.* [12], the initial time $t_{\mathrm{i}}^{(j)} \triangleq t_{0,\mathrm{k}}^{(j)}$ of the generic jth kick phase is reset to 0 s, $j \in \mathbb{N} = \{1, 2, 3, \ldots\}$) and $v_{\mathrm{ramp}}(t_{0,\mathrm{k}}^{(j+1)}) = 0\,\mathrm{V}$, because the initial condition of the voltage across the capacitor C_{ramp} is set to 0 V, and the voltage source v_{+} is only applied for $t \geq t_{0,\mathrm{k}}^{(j+1)}$. The following inverting op amp stage in Figure 4(e) allows to compare the constant voltage v_{a} in Equation 34 with the ramp signal $v_{\mathrm{ramp}}(t)$ in Equation 35. Its output is computed through

$$v_{\mathrm{out}}(t) = -\frac{R_{\mathrm{add3}}}{R_{\mathrm{add1}}}v_{\mathrm{a}} - \frac{R_{\mathrm{add3}}}{R_{\mathrm{add2}}}v_{\mathrm{ramp}}(t). \tag{36}$$

Using Equation 35 and letting $R_{\mathrm{add1}} = R_{\mathrm{add2}} = R_{\mathrm{add3}}$, the expression for $v_{\mathrm{out}}(t)$ may be recast as

$$v_{\mathrm{out}}(t) = -v_{\mathrm{a}} + K_{\mathrm{ctrl}}v_{+}t, \tag{37}$$

where we set $K_{\mathrm{ctrl}} = 1/(R_{\mathrm{ramp}}C_{\mathrm{ramp}})$. Now, the $(j+1)$th kick phase goes on so long as $v_{\mathrm{out}}(t)$ keeps the same sign. At the time instant $t = t_{\mathrm{f,k}}^{(j+1)}$ when the two addends in Equation 37 have the same modulus, i.e. when

$$\begin{aligned} t_{\mathrm{f,k}}^{(j+1)} &= \frac{1}{K_{\mathrm{ctrl}}v_{+}}v_{\mathrm{a}} \\ &= \frac{1}{K_{\mathrm{ctrl}}v_{\mathrm{ctrl,max}}}v_{\mathrm{int2}}(t_{\mathrm{f,c}}^{(j)}) \end{aligned} \tag{38}$$

where we used the expression for v_{a} in Equation 34 and the afore-given formula for v_{+}, no further motor control is carried out, and the fly phase commences (Equation 38 is identical to Equation (32) in the part I paper [12]). With reference to Figure 1(a), at time instant $t_{\mathrm{f,k}}^{(j+1)}$ in the $(j+1)$ run of the KFC control strategy, the switch S_3 disconnects the control voltage source v_{ctrl} from the armature node A, while the switch S_2 is flipped to its lowest position so as to allow a continuous monitoring of the armature voltage v_{A}.

Before proceeding with the circuit-theoretic model of the fly phase of the proposed strategy, let us briefly cover the implementation of the initialisation phase. The reasoning is analogue to the one explained earlier for a general catch phase. In fact, the initialisation phase consists of the application of the old GAF paradigm. The only difference with the standard GAF strategy lies in the fact that in the initialisation phase the first inverting integrator output voltage is integrated again with a positive integration constant in order to estimate the duration of the kick phase in a later first application of the KFC control paradigm. The computation of this first estimate is implemented in circuit form in the following way. First, a current expressed by Equation 26 is let flow through the memristor in Figure 4 (a) throughout the initialisation phase. The memristor charge at the end of the GAF strategy application is then read throughout the first kick phase by the circuit shown in plot (b) of Figure 4. This read is expressed by

$$q_{\mathrm{m}}(t_{\mathrm{f,g}}^{(0)}) = q_{\mathrm{m}}(t_{0,\mathrm{g}}^{(0)}) + \frac{1}{R_{\mathrm{i}}}\int_{t_{0,\mathrm{g}}^{(0)}}^{t_{\mathrm{f,g}}^{(0)}} v_{\mathrm{int1}}(t')dt', \tag{39}$$

DOI: 10.1002/cta

with $q_{\mathrm{m}}(t_{0,\mathrm{g}}^{(0)}) = 0\,\mathrm{C}$. Following the same procedure outlined earlier, the circuit in plot (d) of Figure 4 outputs the following voltage during the whole first kick phase

$$v_{\mathrm{a}} = \rho\, K_{\mathrm{int},2} \int_{t_{0,\mathrm{g}}^{(0)}}^{t_{\mathrm{f,g}}^{(0)}} v_{\mathrm{int1}}(t')dt', \tag{40}$$

which, using

$$v_{\mathrm{int2}}(t_{\mathrm{f,g}}^{(0)}) = v_{\mathrm{int2}}(t_{0,\mathrm{g}}^{(0)}) + K_{\mathrm{int2}} \int_{t_{0,\mathrm{g}}^{(0)}}^{t_{\mathrm{f,g}}^{(0)}} v_{\mathrm{int1}}(t')dt', \tag{41}$$

i.e. Equation 26 of the part I companion paper [12], may be finally cast as

$$v_{\mathrm{a}} = \rho\, v_{\mathrm{int2}}(t_{\mathrm{f,g}}^{(0)}). \tag{42}$$

because $v_{\mathrm{int2}}(t_{0,\mathrm{g}}^{(0)}) = 0\,\mathrm{V}$. Finally, analysing the circuit of Figure 4(e), also active throughout the first kick phase, the time at which its output voltage goes to 0 V during the first kick phase may be calculated as follows:

$$t_{\mathrm{f,k}}^{(1)} = \frac{1}{K_{\mathrm{ctrl}} v_{\mathrm{ctrl,max}}} v_{\mathrm{int2}}(t_{\mathrm{f,g}}^{(0)}), \tag{43}$$

which is equivalent to Equation 28 of the part I companion paper [12]. At this instant, the first fly phase is commenced.

Figure 5 illustrates the circuit detecting the time instant $t_{\mathrm{f,f}}^{(j+1)}$ at which the $(j+1)$th fly phase should be terminated (unlike the circuit implementation of the catch phase, where the case $j = 0$ had to be treated separately, the value for j lies here in $\mathbb{N}_0 = \{0, 1, 2, 3, \ldots\}$). The time detection operation revolves around the monitoring of the modulus and polarity of the voltage v_{A} at the armature node A. Because in the fly phase, the armature voltage coincides with the electromotive force v_{ind} falling across the motor terminals, where the latter is expressed by $v_{\mathrm{ind}} = c\,\varphi\,\omega$, this monitoring procedure indirectly allows the observation of modulus and sign of the pendulum axial velocity v, related to the angular velocity ω via equation $v = \omega \cdot |\vec{r}|$, with $\vec{r}$ representing the pendulum load position vector [12]. The switch S_4 in the sample-and-hold circuit of Figure 5 (b) are controlled by a pulse generator v_{sah}, shown in Figure 5 (a). When $v_{\mathrm{sah}} = 1\,\mathrm{V}$ during a $\Delta t_{\mathrm{sample}}$-long sample phase, S_4 is set in the upper configuration, as shown in plot (b), the first voltage follower K_1 transfers the voltage v_{sample} at its input, i.e. the armature node voltage v_{A}, to the top terminal of capacitor C_{sah}, and, coincidentally, the second voltage follower K_2 copies the voltage $v_{C_{\mathrm{sah}}}$ across C_{sah} to the output node. When $v_{\mathrm{sah}} = 0\,\mathrm{V}$ over the subsequent Δt_{hold}-long-hold phase, S_4 is set to the complementary configuration, and the voltage at the output node, referred to as v_{old}, stores the last sample of the circuit input voltage v_{sample}, which is equivalent to the armature voltage v_{A}. Over this hold phase, the hybrid analog-digital circuit of Figure 5(c) is active. The inputs to this circuit are the fixed value of the voltage v_{old} at the output of the sample-and-hold circuit in Figure 5(a) at the end of the sample phase – i.e. the old sample of the armature voltage – and the current input voltage to the sample-and-hold circuit $v_{\mathrm{sample}}(t)$ – i.e. the current armature voltage $v_{\mathrm{a}}(t)$ – which, meanwhile, keeps varying with time, because the fly phase is ongoing. The first analogue stage consists of a couple of comparators, K_3 and K_4. The first (second) one saturates to the positive supply level if the armature voltage is increasing (has positive sign). The second digital stage is composed of three gates, namely, D_1, an AND gate, D_2, a NOR gate and D_3, an OR gate. The output voltage v_{fly} is found to be equal to the positive supply level if the armature voltage is increasing with positive sign (here, the pendulum has passed over the upright position and is descending from the other side of the x axis, see Figure 1(c)), or if the armature voltage is decreasing with negative sign (here, the pendulum has stopped before reaching the target upright position and is starting its descent from the same side of the x axis, see Figure 1(c)). When the output voltage v_{fly} of the circuit of Figure 5(c) is high, the fly phase is terminated, and a new catch phase commences (with reference to Figure 1(a), the switch $S_{\text{kick-fly}}$ is flipped to its centre position to trigger a sensing operation of the $(j+1)$th catch phase).

DOI: 10.1002/cta

4.1. Time-saving, energy-efficient and adaptive ideal memristor-based control

The circuit model of the motor-pendulum system under KFC control with an ideal memristor is the collection of circuits shown in Figures 2, 3, 4 and 5. In the simulations presented in this section, the ideal memristor emulator parameters are set as reported in Table I.

For the simulations on the ideal emulator-based KFC strategy presented in the next section, the emulator parameter values were chosen as reported in Kim *et al.* [14], i.e. as established by constraints (13) and (14), apart from the capacitance, which is 100 times higher here. For the capacitance value reported in Kim *et al.* [14], the memristor-based integration of the first inverting integrator output voltage v_{int1} would have been too fast for the application at hand without further impractical circuit modifications.

Regarding the initial conditions for the overall system, as explained in the part I paper [12], at the start of each KFC strategy application, the current i_1 through resistor R_1 in Figure 4(b) from Ascoli *et al.* [12], proportional to the pendulum angular velocity ω, the current i_{A} through resistor R_{A} in Figure 5(b) from Ascoli *et al.* [12], modelling the armature current i_{A} and the voltage v_{int1} across capacitor C_1 in Figure 5(c) from Ascoli *et al.* [12], denoting the first inverting integrator output voltage v_{int1}, are all set to zero. Further, the voltage v_{C} across capacitor C_{pos} in Figure 4(c) from Asscoli *et al.* [12], proportional to the pendulum angle γ, is set for comparison purposes to the same value, i.e. 3.04, as in the corresponding simulations on the application of the GAF paradigm in Ascoli *et al.* [12]. Moreover, the initial condition for the voltage $v_{\mathrm{C_{sah}}}$ across capacitor C_{sah} is set to zero. Finally, noting that, from Equations 26, 32 and 34, the initial condition for the second non-inverting integrator output voltage at the beginning of the $(j+1)^{\mathrm{th}}$ ($j \in \mathbb{N} = \{1, 2, 3, \ldots\}$) strategy run may be expressed as

$$\begin{aligned} v_{\mathrm{int2}}(t_{\mathrm{i}}^{j+1}) &= K_{\mathrm{int2}}\, R_{\mathrm{i}} \left(\int_{t_{0,\mathrm{g}}^{(0)}}^{t_{0,\mathrm{c}}^{(j)}} i_{\mathrm{m}}(t')dt' + \int_{t_{0,\mathrm{c}}^{(0)}}^{t_{\mathrm{f,c}}^{(j)}} i_{\mathrm{m}}(t')dt' \right) \\ &= K_{\mathrm{int2}}\, R_{\mathrm{i}}\, q_{\mathrm{m}}(t_{\mathrm{f,c}}^{(j)}), \end{aligned} \tag{44}$$

it is clear that the value for v_{int2} at time instant t_{i}^{j+1}, which is reset to 0 s as should be clear by now, is proportional to $q_{\mathrm{m}}(t_{\mathrm{f,c}}^{(j)})$, which corresponds to the time history of the current flowed through the memristor up to the final time instant $t_{\mathrm{f,c}}^{(j)}$ of the preceding jth catch phase (observe that $q_{\mathrm{m}}(t_{\mathrm{i}}^{(j+1)}) \equiv q_{\mathrm{m}}(t_{\mathrm{f,c}}^{(j)})$ thanks to the non-volatility property of the ideal memristor [9]).

Before the first application of the KFC paradigm, the old GAF strategy is carried out once on the motor-pendulum system with a rod of nominal length $l = 10$cm loaded with a mass of nominal mass $m = 10$ g. This preliminary initialisation phase allows the determination of an initial estimate for the time instant $t_{\mathrm{f,k}}^{(1)}$ at which the fly phase in the first application of the KFC strategy should commence. Regarding the initialisation phase, the initial conditions for the aforementioned circuit variables i_1, i_{A}, v_{int1}, v_{C} and $v_{\mathrm{C_{sah}}}$ keep unchanged with respect to each successive run of the KFC strategy, whereas the charge through the memristor at $t_{\mathrm{i}}^{(0)}$ is set to 0 C, implying a null starting value for $v_{\mathrm{int2}}(t_{\mathrm{i}}^{(0)})$. Observe that from Table I, a null value for $q_{\mathrm{m}}(t_{\mathrm{i}}^{(0)})$ implies that the initial memristance of the emulator in the initialisation phase is $R(q_{\mathrm{m}}(t_{\mathrm{i}}^{(0)})) = R_{\mathrm{s}} = 16\,\mathrm{k}\Omega$.

The initial memristance for the initialisation phase is a design parameter. For positive 'kicks' delivered to the system and under the use of the decremental emulator of Figure 2, a reasonable choice for the initial memristance is its maximum possible value, because the pendulum lift via the application of the old GAF paradigm shall lead to its significant decrease, and the minor adjustments over successive catch phases in later applications of the proposed KFC strategy would not result in its saturation to the upper or lower levels of $R_{\mathrm{off}} = R_{\mathrm{s}} = 16\,\mathrm{k}\Omega$ and R_{on} (in principle equal to $0\,\mathrm{k}\Omega$, see Equation 4), respectively.

Figure 6(a) shows the time evolution of the angle γ, which is basically equivalent to the case shown in Figure 6(b) in the part I paper [12]. Importantly, the memristor-based integration of the voltage v_{int1} during the whole simulation time leads to a considerable decrease in the memristance $R(q_{\mathrm{m}}(t))$ from the aforementioned initial value to a final value of $R(q_{\mathrm{m}}(t_{\mathrm{f,g}}^{(0)})) = 7.6\,\mathrm{k}\Omega$, as shown in Figure 6(b) and clear from its analytical expression, i.e.

DOI: 10.1002/cta

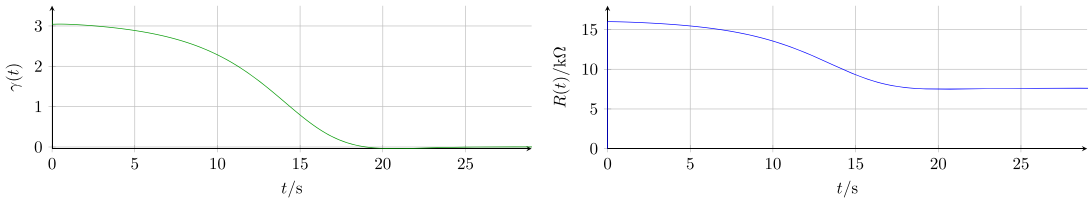

(a) (b)

Figure 6. Initialisation phase of the ideal memristor emulator-based Kick-Fly-Catch control strategy: LTSpice simulation of the circuit model of the overall dynamic system – refer to Figure 3 and to Figures 2, 4 and 5 for the topologies of all circuits in the model – showing the time evolution of the angle γ (a), and the coincidental change in the emulator memristance $R(q_m)$ induced by the non-inverting integration of the first inverting integrator output voltage v_{int1} throughout the simulation time (b). The circuit model accounts for a pendulum of length $l = 10\,\text{cm}$ and mass $m = 10\,\text{g}$ and for the following initial conditions: $\gamma(t_i^{(0)}) = 3.04$, $\omega(t_i^{(0)}) = 0\,\text{rad/s}$, $i_A(t_i^{(0)}) = 0\,\text{A}$, $v_{int1}(t_i^{(0)}) = 0\,\text{V}$ and $v_{int2}(t_i^{(0)}) = 0\,\text{V}$. The angle γ keeps above zero during the whole simulation time. [Colour figure can be viewed at wileyonlinelibrary.com]

$$R(t) = R_s - k_{conv,8}\frac{R_T}{C_T}\int_{t_{0,g}^{(0)}}^{t_{f,g}^{(0)}} \frac{v_{int1}(t')}{R_i}dt', \tag{45}$$

derived from Equations 4 and 39, when one takes into account that for $\gamma \in [0, \pi]$, the first inverting integrator output voltage v_{int1} is positive at all times during the application of the GAF strategy [12]. The value of the memristance at the end of the initialisation phase corresponds to a memristor charge $q(t_{f,g}^{(0)})$ of value

$$q(t_{f,g}^{(0)}) = \left(R_s - R(t_{f,g}^{(0)})\right)\frac{C_T}{k_{conv,8}R_T}, \tag{46}$$

as obtained from (4). It is important to remind at this stage that the second non-inverting integrator output voltage at the beginning of the first KFC strategy run, given by Equation 44 with $j = 0$, i.e.

$$\begin{aligned} v_{int2}(t_i^1) = v_{int2}(t_{f,g}^{(0)}) &= K_{int2}\,R_i\int_{t_{0,g}^{(0)}}^{t_{f,g}^{(0)}} i_m(t')dt' \\ &= K_{int2}\,R_i\,q_m(t_{f,g}^{(0)}), \end{aligned} \tag{47}$$

where $q_m(t_i^{(1)}) = q_m(t_{f,g}^{(0)})$, $t_i^{(0)} \triangleq t_{0,g}^{(0)}$, while $t_i^{(1)} \triangleq t_{0,k}^{(1)}$, is only an estimate for the 'work' to be carried out to raise the pendulum from the initial state to the upright position. As such, an optimisation algorithm needs to be run offline directly at the end of the initialisation phase to scale this estimate empirically so as to obtain the best possible 'kick' in the first application of the proposed KFC control strategy. More specifically, the optimal value for the positive integration constant K_{int2} depends critically upon the dynamics of the memristor-based integration, under the given design parameters, including the pendulum geometric properties (mass m and length l in our model) and the dynamic system initial conditions in the initialisation phase, including $R(t_i)$. With the chosen ideal memristor emulator and under the aforementioned simulation and initial condition settings, the offline tuning procedure directly following the initialisation phase provided an optimal value for K_{int2} equal to $0.36\,\text{s}^{-1}$ (because $k_{conv,8} = 1\,\text{V}^{-1}$, this implies an optimal value for $k_{conv,9}$ equal to $0.36\,\text{V}^2\,\text{s}^{-1}$ and consequently, for the resistance R_a in the circuit of Figure 4(d), according to Equation 31). With the optimal choice for K_{int2}, a scaled version of the value for $v_{int2}(t_i^1)$ from Equation 47 (with scaling factor ρ, see Equation 42, and note that $v_{int2}(t_i^{(1)}) \equiv v_{int2}(t_{f,g}^{(0)})$) shall then be available at the output of the circuit of Figure 4(d) throughout the kick phase in a later first application of the KFC strategy and shall be used coincidentally in the circuit of Figure 4(e) to determine the time $t_{0,f}^{(1)}$ at which the first fly phase shall commence (refer to Equation 55 and recall that $t_{f,k}^{(1)} = t_{0,f}^{(1)}$). The circuit parameters for the circuit of Figure 3 are given in Table I of the companion part I paper [12], except for the maximum control voltage applied to the armature node A during a kick phase, which is set to the positive supply level v_{B+} in the control circuit, i.e.

DOI: 10.1002/cta

Table II. Parameter values for the circuits of Figure 4. R_i scales the first inverting integrator output voltage v_{int1} to provide the current flowing through the memristor and modulating its memristance throughout a catch phase, refer to Figure 4(a). The memristance is then read by the circuit of Figure 4(b) during the following kick phase, when the memristor acts merely as a nonlinear resistor. The value for the reference resistor R_{ref} in the circuit of Figure 4(c) is set to the same value as the resistor R_s in the memristor model. Most importantly, the optimal choice for K_{int2} – see the text for details – resulted in the selection of a resistance R_a of value 110 Ω. The operational amplifiers in Figures 4 (d) and (e) are ideal components available in LTSpice with supply levels set to $\pm v_{B+}$ (note that the maximum control voltage level is chosen as the positive supply level, i.e. $v_{ctrl,max} = v_{B,+}$ [12]). Because $\rho = v_+/v_{ctrl,max}$, its numerical value is $1/9$.

Parameter	Value	Parameter	Value
i_{read1}	1 μA	R_{ref}	16 kΩ
R_i	110 kΩ	$R_{sub1}, R_{sub2}, R_{sub3}, R_{sub4}$	1 kΩ
R_{amp}	1 Ω	R_a	110 Ω
$v_+ = \frac{v_{B+}}{9}$	1 V	R_{ramp}	100 kΩ
C_{ramp}	10 μF	$R_{add1}, R_{add2}, R_{add3}$	1 kΩ

Table III. Parameter values for the circuit of Figure 5, which adopts ideal operational amplifiers available in LTSpice.

Parameter	Value
C_{sah}	100 μF
$\Delta_{t_{sample}}$	1 ms
$\Delta_{t_{hold}}$	9 ms

$$v_{ctrl,max} = v_{B+} = 9\,V. \tag{48}$$

The values of the parameters of the circuits in Figure 4 and 5 are tabulated in Tables II and III, respectively. Regarding the latter table, it is instructive to observe that Δt_{sample} and for Δt_{hold} were selected numerically equal to Δt_{sense} and for Δt_{drive}, despite distinct choices would have also led to a proper functioning of the end-of-fly-phase detection circuit of Figure 5.

The time-efficient and energy-efficient limb movement resulting from the first application of the KFC control strategy is clearly demonstrated in Figure 7. Plots (a) and (b), (c) and (d) and (e), in which the three phases of the proposed paradigm are clearly marked (the kick and fly phases, respectively, occur over the time intervals $[t_{0,k}^{(1)}, t_{f,k}^{(1)}) = [0\,,\ 835\,)$ ms and $[t_{0,f}^{(1)}, t_{f,f}^{(1)}) = [0.835,\ 1.27)$ s, whereas the initial time of the catch phase is $t_{0,c}^{(1)} = 1.27$ s, and the simulation final time was set to 4.5 s), respectively, show the time waveforms of the control voltage v_{ctrl}, of the first integrator output voltage v_{int1} and of the emulator memristance‖ $R(t)$, of the angle γ and of the cost function C computed via

‖The memristance reading during the first kick phase does not corrupt significantly the state of the memristor. In fact, the relative memristance change in the first kick phase, defined as $(R(t_{f,k}^{(1)}) - R(t_{0,k}^{(1)}))/R(t_{0,k}^{(1)})$, with $R(t_{0,k}^{(1)}) = R(t_{f,g}^{(0)}) = 7.6\,\text{k}\Omega$ and $R(t_{f,k}^{(1)}) = 7.55\,\text{k}\Omega$, respectively, denoting the memristance values before and after the reading operation, was found to be equal to −0.66%.

DOI: 10.1002/cta

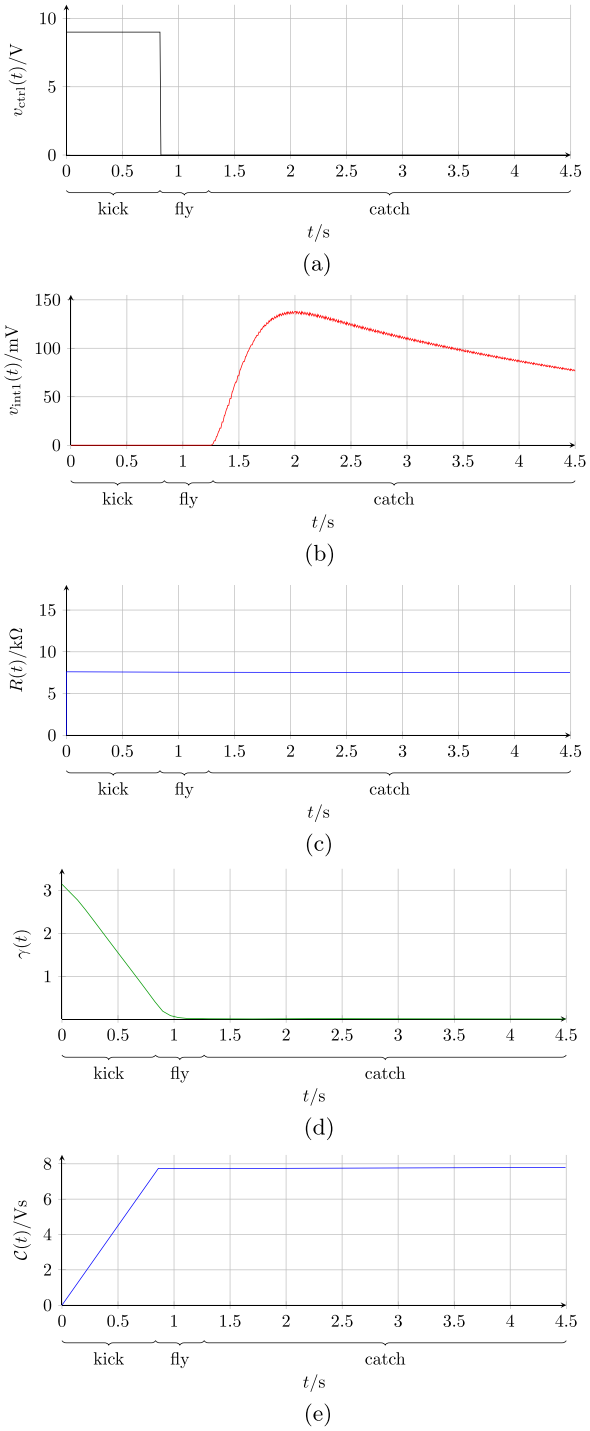

Figure 7. First application of the ideal memristor emulator-based Kick-Fly-Catch control paradigm to an inverted pendulum with a load of length $l = 10\,\mathrm{cm}$ and a mass m of 10 g after the initialisation phase illustrated in Figure 6: LTSpice simulation of the circuit model of the overall dynamic system showing the time evolution of the control voltage v_{ctrl} (a), of the first integrator output voltage v_{int1} (b), of the emulator memristance $R(t)$ (c), of the angle γ (d) and of the cost function $\mathcal{C}$ (e). The three phases of the Kick-Fly-Catch strategy are clearly marked on the five diagrams. The circuit model accounts for the following initial conditions: $\gamma(t_{\mathrm{i}}^{(1)}) = 3.04$, $\omega(t_{\mathrm{i}}^{(1)}) = 0\,\mathrm{rad/s}$, $i_{\mathrm{A}}(t_{\mathrm{i}}^{(1)}) = 0\,\mathrm{A}$, $v_{\mathrm{int1}}(t_{\mathrm{i}}^{(1)}) = 0$ and $v_{\mathrm{int2}}(t_{\mathrm{i}}^{(1)}) = v_{\mathrm{int2}}(t_{\mathrm{f,g}}^{(0)})$. The enforcement of the latter initial condition exploits the use of a nonvolatile memory cell with initial memristance $R(t_{\mathrm{i}}^{(1)}) = R(t_{\mathrm{f,g}}^{(0)})$. [Colour figure can be viewed at wileyonlinelibrary.com]

DOI: 10.1002/cta

$$C(t) = \int_{t|_{\gamma=\gamma(t_{\mathrm{i}}^{(1)})}}^{t|_{\gamma=\gamma(t)}} |v_{\mathrm{A}}(t')|dt', \tag{49}$$

where $\gamma_{t_{\mathrm{i}}^{(1)}} = \gamma(t_{0,\mathrm{k}}^{(1)})$ represents the pendulum angle at the beginning of the first application of the KFC paradigm following the initialisation phase.

As shown in Figure 7(b), the 'kick' delivered to the motor-pendulum system is pretty good here. The angle γ at the end of the kick phase is almost at its target position and moves even closer to zero during the subsequent fly phase. The fly phase is terminated when the pendulum stops moving up and starts its descent from the same side of the x axis (refer to Figure 1(c)). The first sense phase in the catch process will thus produces a positive increase in v_{int1} from its starting value of $v_{\mathrm{int1}}(t_{0,\mathrm{c}}^{(1)}) = v_{\mathrm{int1}}(t_{\mathrm{i}}^{(1)}) = 0\,\mathrm{V}$, as illustrated in Figure 7(b). In the first drive phase, the application to the armature node of the positive DC voltage appearing at the output of the first integrator at the end of the preceding sense phase will not be high enough to induce a motor torque counteracting successfully the gravitation torque. Thus, a further increase in the pendulum angle is observed in this first drive phase as well. The monotonous pendulum descents under sensing and driving (not visible in plot (d) of Figure 7 but observable later in the discussion related to the adoption of larger pendulum masses, see Figure 8(a)) with consequent build-up of a positive voltage at the output of the first integrator during sense phases goes on for a while. At some point, the voltage v_{int1} will be large enough to produce a motor torque winning over the gravitation torque, thus inducing the pendulum ascent, over drive phases. The following sense phases witness an initial decrease in the angle γ, driven by the momentum gained by the pendulum in the preceding drive phases, before the gravitation torque forces the pendulum downward motion. As the target position is approached, the reduction in the gravitation torque combined with the increase in the momentum gained by the pendulum in the preceding drive phase (because of the larger voltage applied to the armature node over that phase) determines a net pendulum ascent over each sense phase as well. This will result in a coincidental net decrease in the voltage v_{int1}. The pendulum net ascents under sensing (not visible in plot (d) of Figure 7 but observable later in the discussion related to the adoption of larger pendulum masses, see Figure 8(a)) with consequent net reduction in the positive voltage at the output of the first integrator during sense phases goes on till the pendulum attains the upright position, and v_{int1} converges to the null value (this happens later than the final simulation time, refer to Figure 7(d)). Afterwards, the pendulum angle and the first integrator output voltage are found to undergo small oscillations around their target null values.

Looking at Figure 7(c), it may be noticed that the memristance does not undergo noticeable changes during the first catch phase, implying that the estimate for the following kick phase duration shall not experience major changes either. In fact, provided no significant perturbation is applied to the initial conditions of the dynamic system, and no major modification to the pendulum geometric properties is on the way, the first estimate for the 'kick' phase duration will work rather well in all successive applications of the KFC strategy.

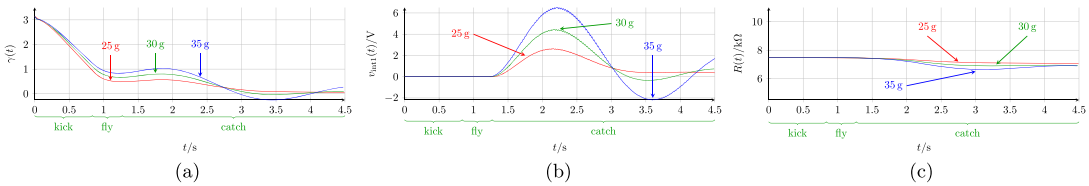

Figure 8. First application of the ideal memristor emulator-based Kick-Fly-Catch control paradigm to an inverted pendulum of length $l = 10\,\mathrm{cm}$ and load mass m different from the original value of 10 g: LTSpice simulation of the circuit-theoretic model of the overall dynamic system showing the time evolution of the angle γ (a) and the changes in the first integrator output voltage v_{int1} (b) and in the emulator memristance R (c) in the catch phase. The curves in red, green and blue refer to a load of mass m equal to 25, 30 and 35 g, respectively. The time intervals of the three phases are clearly highlighted for the load mass $m = 30\,\mathrm{g}$. The starting value of the first integrator output voltage v_{int1} is 0 V. The value of the initial emulator memristance at time $t_{\mathrm{i}}^{(1)} = t_{0,\mathrm{k}}^{(1)}$, common to each of the three scenarios, is equal to the memristance at the end time $t_{\mathrm{f,g}}^{(0)}$ of the initialisation phase conducted on the load with mass $m = 10\,\mathrm{g}$, i.e. $R(t_{\mathrm{f,g}}^{(0)}) = 7.6\,\mathrm{k\Omega}$. [Colour figure can be viewed at wileyonlinelibrary.com]

DOI: 10.1002/cta

The calculation of the time Δt needed to raise the pendulum angle γ from its initial value $\gamma(t_{0,\mathrm{k}}^{(1)}) = 3.04$ to the threshold γ_{th}, set to 0.1, gave a value of

$$\Delta t = t|_{\gamma=\gamma_{\mathrm{th}}} - t|_{\gamma=\gamma(t_{\mathrm{i}})} = 960 \text{ ms}, \tag{50}$$

which is considerably lower than the corresponding measure of 17.8 s attained in the corresponding LTSpice simulation on the circuit-theoretic model of the motor-pendulum system under GAF control [12]. Further, the power consumed to carry out this specific pendulum angle decrease, estimated through the evaluation of the cost function at the time at which γ attains the threshold γ_{th}, was found to be

$$C(t|_{\gamma=\gamma_{\mathrm{th}}}) = 7.74\ Vs. \tag{51}$$

It is significantly reduced as compared with the value of 20.4 Vs determined in the corresponding LTSpice simulation of the motor-pendulum system under GAF control[**] [12].

Very importantly, the proposed KFC strategy exploits the learning capability of the memristor to adapt to changes in the limb topology or to perturbations of the initial conditions of the dynamic system. Suppose that after the initialisation phase illustrated in Figure 6, the pendulum load mass m is increased as compared with the original value of 10 g (three scenarios, corresponding to values for m in the set {25, 30, 35} g, are examined here). Importantly, the positive integration constant K_{int2} for the second non-inverting integrator is kept equal to the value of $0.36\,\mathrm{s}^{-1}$, which was earlier derived through an offline optimisation procedure directly at the end of the initialisation phase to obtain a perfect 'kick' for the motor-pendulum system with a load mass m of 10 g. It follows that the first kick phase duration, fitted to the case of the original pendulum mass, is too short for each of the three scenarios under consideration. As a result, as demonstrated in Figure 8(a), the pendulum angle at the end of the first kick phase is quite distant from the value of 0, being farther away from the target the larger the pendulum load mass. Recalling the discussion on the time behaviours of the first integrator output voltage and of the pendulum angle in the catch phase of the first application of the paradigm to the inverted pendulum system with a load mass of 10 g – see plots (b) and (d) in Figure 7 – for each load mass scenario considered here, within a catch phase γ – see Figure 8(a) – and v_{int1} – see Figure 8(b) – are found to undergo an initial increase, followed by a subsequent decrease towards their target values, with more significant rate of changes the larger the load mass. This is the reason why for $m = 35$ g, the approach of the pendulum angle and of the first inverting integrator output voltage to the null value is not as smooth as in the other two load mass cases or in the optimal scenario described in Figure 7. When the angle goes negative (this is visible for the cases $m = 30$ and 35 g in plots (a) and (b) of Figure 8), the control system operates in a complementary fashion, leading to an initial further decrease in γ and v_{int1}, which subsequently experience a sign-reversed time evolution rate, approaching the null value once again (this time with a reduced overshoot for the largest load mass case, a signature for the stability of the overall system under the proposed strategy).

The memristance in the first catch phase – see Figure 8(c) – evolves with time according to

$$R(t) = R_{\mathrm{s}} - k_{\mathrm{conv},8}\frac{R_{\mathrm{T}}}{C_{\mathrm{T}}}\left(q(t_{0,\mathrm{c}}^{(1)}) + \int_{t_{0,\mathrm{c}}^{(1)}}^{t_{\mathrm{f,c}}^{(1)}} \frac{v_{\mathrm{int1}}(t')}{R_{\mathrm{i}}}dt'\right), \tag{52}$$

where assuming an uncorrupted memristance reading in the first kick phase, $q(t_{0,\mathrm{c}}^{(1)}) \equiv q(t_{\mathrm{f,g}}^{(0)})$ and is, thus, expressed by Equation 46. For $m = 25$ and 30 g, i.e. for all cases where there appears a smooth approach of the pendulum angle to 0, a noticeable change – particularly a decrease – in the memristance within the first catch phase is noticed from the time at which the first integrator output voltage has attained a sufficiently high positive value to induce the pendulum ascent under driving until the time at which the angle and v_{int1} attain the null numerical value (refer to the earlier discussion). In these two load mass scenarios, the memristance of the emulator is not noticeably modulated thereafter. For the case

[**] The energy consumption in the initialisation phase was not taken into account because it is shared among all KFC control strategy runs, so, as the number of runs grows, the initialisation phase-related energy share per KFC strategy application gets more and more negligible.

DOI: 10.1002/cta

of the largest mass, however, because of the overshoot following the zero in the angle time waveform, the memristance experiences a later increase from the time where the negative-valued voltage v_{int1} has attained a sufficiently high modulus to induce the pendulum ascent under driving until the time at which the angle and v_{int1} attain the null numerical value. Afterwards, for m=35g, the resistance of the memristor does not experience further significant changes. Most importantly, the final value of the memristance at the end of this first catch phase is found to be lower the larger the load mass. As a result, the final value of the memristor charge, expressed by

$$q(t_{\mathrm{f,c}}^{(1)}) = \left(R_{\mathrm{s}} - R(t_{\mathrm{f,c}}^{(1)})\right) \frac{C_{\mathrm{T}}}{k_{\mathrm{conv,8}} R_{\mathrm{T}}}, \tag{53}$$

has a higher value the heavier the mass, leading to a larger voltage available at the output of the circuit of Figure 4(d) throughout the second kick phase, i.e. a ρ-scaled version of the second integrator output voltage, expressed, following Equation 44, by

$$\begin{aligned} v_{\mathrm{int2}}(t_{\mathrm{i}}^{2}) &= K_{\mathrm{int2}}\, R_{\mathrm{i}} \left(\int_{t_{0,\mathrm{g}}^{(0)}}^{t_{0,\mathrm{c}}^{(1)}} i_{\mathrm{m}}(t')dt' + \int_{t_{0,\mathrm{c}}^{(1)}}^{t_{\mathrm{f,c}}^{(1)}} i_{\mathrm{m}}(t')dt' \right) \\ &= K_{\mathrm{int2}}\, R_{\mathrm{i}}\, q_{\mathrm{m}}(t_{\mathrm{f,c}}^{(1)}). \end{aligned} \tag{54}$$

Thus, recalling Equation 55 and observing that $v_{\mathrm{int2}}(t_{\mathrm{i}}^{2}) = v_{\mathrm{int2}}(t_{\mathrm{f,c}}^{(1)})$ because $t_{\mathrm{i}}^{2} = t_{0,\mathrm{k}}^{(2)}$, the circuit of Figure 4(e) active throughout the second kick phase, shall output a zero voltage at an instant, expressed by

$$t_{\mathrm{f,k}}^{(2)} = \frac{1}{K_{\mathrm{ctrl}} v_{\mathrm{ctrl,max}}} v_{\mathrm{int2}}(t_{\mathrm{f,c}}^{(1)}), \tag{55}$$

later in time the larger the load mass, contributing to correct the first wrong estimate in each of the three scenarios.

Remark 2
It is instructive to note, at this stage, that under a positive (negative) area under the time waveform of v_{int1} over the 1st catch phase, calling for a lengthening (shortening) of the 2nd kick phase duration, the memristance of the emulator at $t_{\mathrm{f,c}}^{(1)}$ would get smaller (larger) than its value at $t_{0,\mathrm{c}}^{(1)}$ according to Equation 52, implying a higher (lower) final value $q_{\mathrm{m}}(t_{\mathrm{f,c}}^{(1)})$ for the memristor charge with respect to its initial condition $q_{\mathrm{m}}(t_{0,\mathrm{c}}^{(1)})$ in line with Equation 53, resulting in a stretched (shrunk) time span $t_{\mathrm{f,k}}^{(2)}$ for the 2nd kick phase, as follows from Equation 55.

As demonstrated in Figure 9(a), in all load mass cases, the 'longer kick', delivered to the motor-pendulum system by application of the voltage $v_{\mathrm{ctrl,max}} = v_{\mathrm{B,+}}$ to the armature node, reduces the pendulum angle much more than in the first application of the strategy (with γ farther away from the

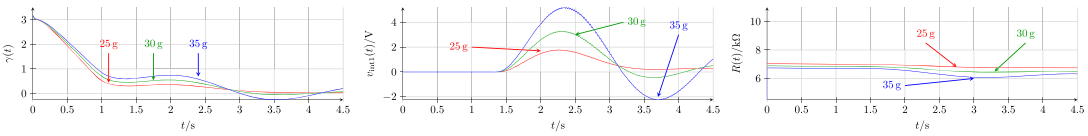

(a) (b) (c)

Figure 9. LTSpice simulation results from the second application of the ideal memristor-based Kick-Fly-Catch strategy to the circuit-theoretic model of the motor-pendulum system with a rod of length $l = 10$ cm and load mass m different from the original value of 10 g. Time evolution of the angle γ (a) variation of the first integrator output voltage v_{int1} (b) and of the emulator memristance R over the catch phase (c). The curves in red, green and blue refer to a load of mass m equal to 25, 30 and 35 g, respectively. The initial condition of the voltage v_{int1} is 0 V. The initial emulator memristance, different for each of the three scenarios, is equal to its value at the end of the catch phase in the first application of the Kick-Fly-Catch paradigm. [Colour figure can be viewed at wileyonlinelibrary.com]

DOI: 10.1002/cta

target null value the larger the load mass, as expected). The oscillations of the first integrator output voltage around 0 V – see plot (b) in Figure 9 – become smaller. This notwithstanding, as shown in Figure 9(c), the emulator memristance, starting with a distinct initial condition $R(t_{\mathrm{i}}^{(2)}) = R(t_{\mathrm{f,c}}^{(1)})$ depending upon m (refer to Fig. 8(c)), still undergoes some change over the catch phase, attaining a lower value the larger the load mass. It follows that the kick phase in a third application of the proposed strategy would be longer the larger the load mass, reducing the error in the kick duration estimate for each of the three scenarios.

After a small number of runs n – assuming values in the set $\{4, 5, 6\}$ for a pendulum load of mass m in the set $\{25, 30, 35\}$g, respectively –, the 'kick' delivered to the system is optimal, as demonstrated in Figure 10: the angle at the end of the kick phase is very close to the target value (plot (a), highlighting the considerable reduction in pendulum lift time over the precorrection case illustrated in Figure 8(a)), the oscillations of the first integrator output voltage v_{int1} around 0 V are becoming smaller (plot (b)), and the memristance undergoes practically no change over the catch phase (plot (c)).

Similar results on the adaptable nature of the proposed control approach are obtained by increasing the rod length l rather than the load mass m as compared with its nominal value of 10 cm after the initialisation phase conducted on the original system (refer to Figure 6). Two scenarios, corresponding to a pendulum with length l in the set $\{15, 20\}$ cm, are investigated. Keeping $K_{\mathrm{int2}} = 0.36$ 1/s, as derived through an offline optimisation procedure carried out directly at the end of the initialisation phase and fitted to a pendulum with length $l = 10$ cm and load mass $m = 10$ g, the resulting kick phase duration in the first application of the KFC strategy – see Figure 11(a) – results to be too short for each of the two scenarios under interest, especially for the longer rod case. In both scenarios, the emulator memristance

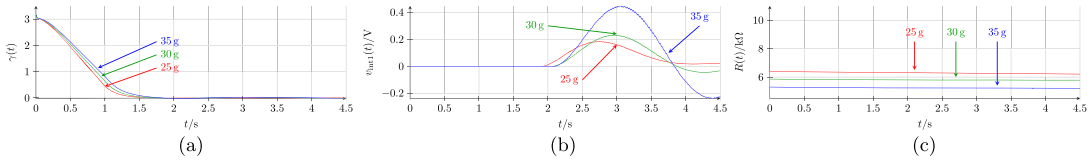

Figure 10. LTSpice simulation of the circuit-theoretic model of the overall dynamic system under the nth application of the ideal memristor emulator-based Kick-Fly-Catch (KFC) paradigm to an inverted pendulum of length $l = 10$ cm and load mass m different from the original value of 10 g: time evolution of the angle γ (a), of the first integrator output voltage v_{int1} (b) and of the emulator memristance R (c). The curves in red, green and blue refer to a load of mass m equal to 25, 30 and 35 g, respectively. The initial voltage at the output of the first integrator is set to 0 V. The initial emulator memristance, different for each of the three scenarios, is equal to its value at the end of the catch phase in the $(n-1)$th application of the KFC paradigm. The iteration number n is equal to 4, 5 and 6 for the load of mass 25, 30 and 35 g, respectively. For each load mass scenario, the time integration of v_{int1} produces no visible change in the emulator memristance in the catch phase, resulting in an optimal kick phase duration estimate for a later application of the KFC control strategy. [Colour figure can be viewed at wileyonlinelibrary.com]

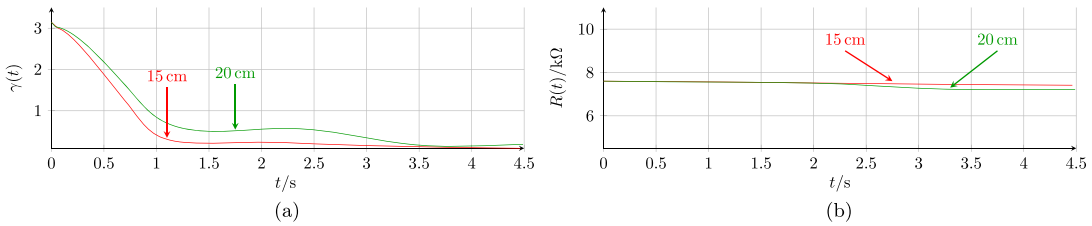

Figure 11. First application of the ideal memristor emulator-based Kick-Fly-Catch control paradigm to an inverted pendulum of load mass $m = 10$ g and length l different from the original value of 10 cm. LTSpice simulation of the circuit-theoretic model of the overall dynamic system showing the time evolution of the angle γ (a) and the change in the emulator memristance in the catch phase (b). The curves in red and green refer to a rod of length l equal to 15 and 20 cm, respectively. The value of the initial emulator memristance at time $t_{\mathrm{i}}^{(1)} = t_{\mathrm{0,k}}^{(1)}$, common to each of the two scenarios, is equal to the memristance at the end time $t_{\mathrm{f,g}}^{(0)}$ of the initialisation phase conducted on the pendulum with length $l = 10$ cm, i.e. $R(t_{\mathrm{f,g}}^{(0)}) = 7.6\,\mathrm{k\Omega}$. [Colour figure can be viewed at wileyonlinelibrary.com]

DOI: 10.1002/cta

experiences some change over the catch phase – see Figure 11(b) – attaining a lower final value for the longer pendulum case. This allows to stretch the duration of a second kick phase on the basis of the pendulum length. As shown in Figure 12(a), for both scenarios, the pendulum angle gets closer to zero over the second kick phase, remaining farther away from the target value for the longer rod, as expected. The emulator memristance undergoes less significant changes over the second catch phase – clearly visible only for $l = 20\,\text{cm}$ in Figure 12(b) – but its final value, lower for the longer pendulum, allows to increase the next kick phase duration according to the value for l. After just four strategy runs, the 'kick' is optimal for both scenarios, as demonstrated in Figure 13. In each rod length case, the pendulum approaches the upright position already over the kick phase (plot (a)), resulting in an uncorrupted emulator memristance over the catch phase.

Further extensive simulations have been carried out on the circuit-theoretic model of the motor-pendulum system under KFC strategy. The investigations covered the case where after the initialisation phase fitted to the original pendulum geometry, the load mass or the rod length were decreased as compared with their nominal values. Because the ideal memristor emulator integration works in a perfectly symmetrical fashion on integrand functions of opposite polarities, the dynamic system achieves similarly high performance levels as in the scenarios examined earlier. Here, the adaptive nature of the control system leads to a progressive decrease in the duration of the kick phase. The optimal 'kick' was found to be shorter for lower values of the load mass or of the rod length, as expected.

Remark 3

As a final note, throughout this manuscript, the discussion on the KFC strategy has assumed a positive-signed 'kick' control voltage $v_{\text{ctrl}} = v_{\text{ctrl,max}} \in \mathbb{R}_+$, leading to a decrease in the pendulum angular position from $\gamma = \pi$ towards $\gamma = 0$. A similar analysis may be applied *mutatis mutandis* to the case

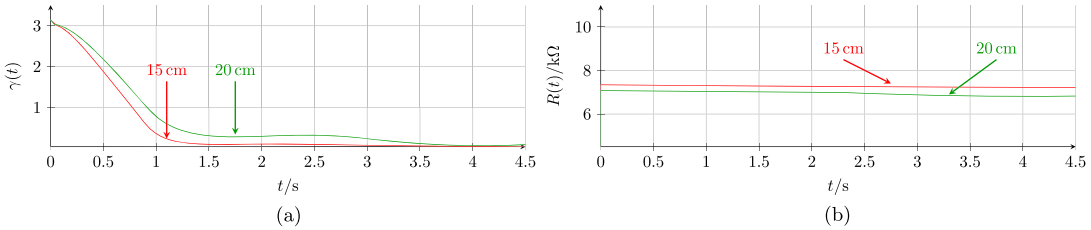

Figure 12. Second application of the ideal memristor emulator-based Kick-Fly-Catch control paradigm to an inverted pendulum of load mass $m = 10\,\text{g}$ and length l different from the original value of 10 cm: LTSpice simulation of the circuit-theoretic model of the overall dynamic system showing the time evolution of the angle γ (a) and the change in the emulator memristance in the catch phase (b). The curves in red and green refer to a rod of length l equal to 15 and 20 cm, respectively. The initial emulator memristance at time $t_{\text{i}}^{(2)} = t_{0,\text{k}}^{(2)}$, distinct for each of the two scenarios, is equal to the memristance value at the final time $t_{\text{f,c}}^{(1)}$ of the first catch phase. [Colour figure can be viewed at wileyonlinelibrary.com]

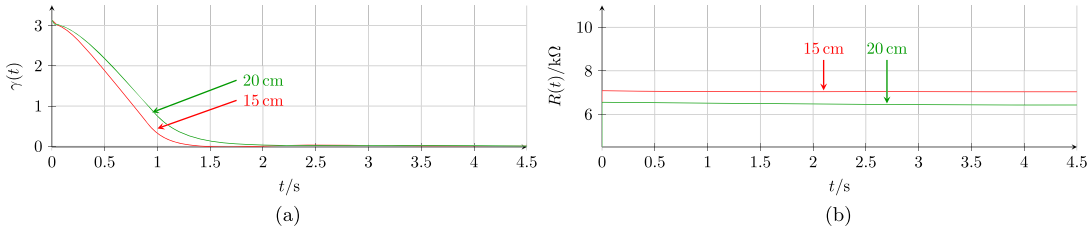

Figure 13. Fourth application of the ideal memristor emulator-based Kick-Fly-Catch control paradigm to an inverted pendulum of load mass $m = 10\,\text{g}$ and length l different from the original value of 10 cm. LTSpice simulation of the circuit-theoretic model of the overall dynamic system showing the time evolution of the angle γ (a) and the change in the emulator memristance in the catch phase (b). The curves in red and green refer to a rod of length l equal to 15 and 20 cm, respectively. The initial emulator memristance at time $t_{\text{i}}^{(4)} = t_{0,\text{k}}^{(4)}$, distinct for each of the two scenarios, is equal to the memristance value at the final time $t_{\text{f,c}}^{(3)}$ of the third catch phase. [Colour figure can be viewed at wileyonlinelibrary.com]

DOI: 10.1002/cta

of a negative-signed 'kick' control voltage $v_{\text{ctrl}} = v_{\text{ctrl,min}} = -v_{\text{ctrl,max}} \in \mathbb{R}_-$, which would raise the pendulum from the negative side of the x axis (refer to Figure 1(a)), i.e from $\gamma = -\pi$ towards $\gamma = 0$. One aspect is worth mentioning regarding the circuit-theoretic model under negative 'kicks'. Here, the circuits contributing to detect the final time instant for a kick phase reported in Figures 4 may be kept unchanged provided the decremental emulator from Kim *et al.* [14], reported in Figure 2, is replaced by the incremental emulator illustrated in Figure 3(a) from Kim *et al.* [14]. In fact, in this case, it is necessary that, over an adaptive catch phase, a negative (positive) voltage v_{int1} at the output of the inverting integrator, calling for a longer (shorter) kick phase duration in the following application of the KFC strategy, would simultaneously induce a decrease (increase) of the device memristance. Once again, the emulator memristance at the beginning of the initialisation phase is set to the maximum value $R(t_{\text{i}}) = R(t_{0,\text{g}}^{(0)}) = R_{\text{off}} = R_{\text{s}} = 16\,\text{k}\Omega$. Under negative 'kicks,' it is also possible to use the decremental memristor configuration of Figure 2, but in that case, the circuit of Figure 4 should be modified so that a longer (shorter) kick phase duration estimate for the next KFC strategy run would result from an increase in the memristance during the current catch phase. Furthermore, in that case, the initial condition on the memristance at the beginning of the initialisation phase would be set to $0\,\Omega$, implying a non-zero initial value for q_{m} at the same time. As a result, because $v_{\text{int2}}(t_{\text{i}})$ has to be equal to 0 V, further design considerations should be laid down to uncouple the initial conditions on memristor charge and second non-inverting integrator output voltage.

The next section shall first introduce a circuit-theoretic model of the motor-pendulum system under the proposed KFC paradigm based upon the model [15] of a real nanoscale memristor fabricated at Knowm Inc. [16] revisited in Section 3.2) and then shall discuss the performance levels of the given circuit implementation on the basis of LTSpice simulations.

5. KNOWM MEMRISTOR-BASED CIRCUIT-THEORETIC MODEL OF THE KFC PARADIGM

Here, the model [15] of the real memristor device from Knowm, Inc. [16] – see Section 3.2 – is adopted to present a more practical circuit realisation of the novel KFC control strategy. A deep analysis of the performance of the real memristor device as signal integrator was carried out through the run of extensive numerical simulations of its model. The study revealed that the physical memristor from Knowm, Inc. does not perform an accurate time integration operation as far as the accuracy requirements of the application under study is concerned[††]. The next section gains a deeper insight into this crucial point.

5.1. Integrator performance of the Knowm memristor

The parameter values of the MSS memristor model from Section 3.2 are reported in Table IV. Note that, because a unitary value is attributed to parameter ϕ, the memristor current i_m has no Schottky diode component here. Further, it is instructive to point out that the maximum and minimum conductances of the device are expressed by $G_{\text{max}} = N_{\text{tot}} G_2 = 3\,\text{mS}$, corresponding to the on-resistance $R_{\text{on}} = 333\,\Omega$, and by $G_{\text{min}} = N_{\text{tot}} G_1 = 1\,\mu\text{S}$, corresponding to the off-resistance $R_{\text{off}} = 1\,M\Omega$, respectively.

The MSS model of the voltage-controlled Knowm memristor is non-deterministic. This on its own impairs its performance as signal integrator. Nevertheless, the possibility of using the device as integrator shall be examined in the subsequent text.

The intuitive approach to analogue signal integration, consisting in the application of the continuous signal to be processed in voltage form across the memristive one-port ([12], [21]), does not work well for the Knowm memristor. The time, the CSL needs to lift the pendulum from the stable rest state to the

[††] We tested several other models of nanoscale nonvolatile memory cells to investigate the integration performance of real memristors. In all cases, the studies revealed the inability of state-of-the-art nanoscale memristors to act as ideal signal integrators. Particularly, because of the huge variation range, covering several orders of magnitude, of the switching kinetics of physical memristors [20], depending upon initial state and input magnitude, in general, the device response to a continuous-time stimulus does not provide its time integration. With the ever-growing advancement in memristor manufacturing technology, we envision that in the near future that it shall be possible to re-engineer materials so as to tune the electrical properties of the nano-devices to the application of interest, making the fabrication of a memristor-based integrator feasible.

DOI: 10.1002/cta

Table IV. Parameters of the metastable switch memristor model.

Parameter	Value	Parameter	Value
N_{tot}	10^6	ϕ	1
α	$8.3 \cdot 10^{-3}$	$V_{\mathrm{m,1}}$	0.4 V
$V_{\mathrm{m,2}}$	0.3 V	V_{T}	26 mV
G_1	1 pS	G_2	3 nS

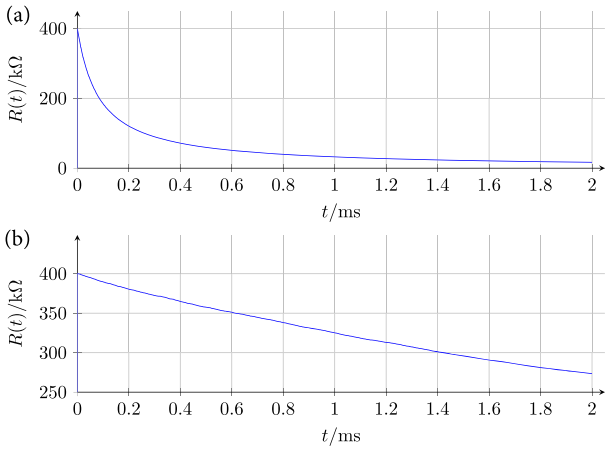

Figure 14. (a) ((b)) Memristance R of the Knowm nano-device over time under pulse train excitation with amplitude 250 (150) mV over the first 500 ns-long half period and 0 V over the second 500 ns-long half period. [Colour figure can be viewed at wileyonlinelibrary.com]

upright position is rather long relatively to the ultra-fast memristive dynamics ([22], [23]). It follows that, as the first integrator output voltage builds up during a catch phase, it is bound to exceed by far the memristor threshold voltage. When this occurs, the memristance is rapidly driven to its maximum or minimum value, without any further change thereafter, unless the voltage across it changes polarity. It seems thus reasonable to use a different methodology to modulate the memristance of the Knowm nano-device over a catch phase. Rather than applying the analogue voltage waveform at the output of the first integrator across its terminals, a train of voltage pulses shaped according to modulus and polarity of the voltage v_{int1} according to the device switching kinetics shall be employed to induce a memristor response as close as possible to a signal integration. After all, the use of pulse-based inputs for memristance programming is standard in the industry [21], e.g., most importantly for the purpose of our research study, for the Knowm device [16]. Figure 14 refers to a LTSpice simulation where the MSS memristor was excited by applying a train of pulses directly across it. The time evolution of the device memristance $R(t)$ from an initial value $R(t_{\mathrm{i}})$ of 400 kΩ under a pulse train stimulus with pulses of period 1 μs and amplitude 250 (150) mV over the first 500 ns-long half cycle and 0 V over the second 500 ns-long half cycle is shown in plot (a) ((b)) of Figure 14 ($t_{\mathrm{i}} = 0$ s). The larger pulse amplitude over the first half cycle of the input pulse train speeds up the device switching kinetics, with the inevitable asymptotic saturation of the memristance to the aforementioned minimum R_{on} value. On the other hand, the memristance response to the input pulse train with lower amplitude over the first half cycle is linear. Thus, the Knowm memristor works as an ideal signal integrator in this case. This investigation suggests that the pulse-based stimulus applied across the real nano-device should be small enough to induce a limited change in the memristance. Under these conditions, in fact, the Knowm memristor acts as a good signal integrator (see plot (b) in Figure 14). This implies that the use of the nano-device to integrate a pulse train stimulus, shaped according to the wide-range voltage at the output of the first inverting integrator throughout a preliminary application of the GAF control paradigm, is inappropriate. The initialisation phase shall then be skipped in the Knowm memristor-based circuit implementation of the KFC control strategy. The initial value of the memristance for the first application of the proposed KFC

DOI: 10.1002/cta

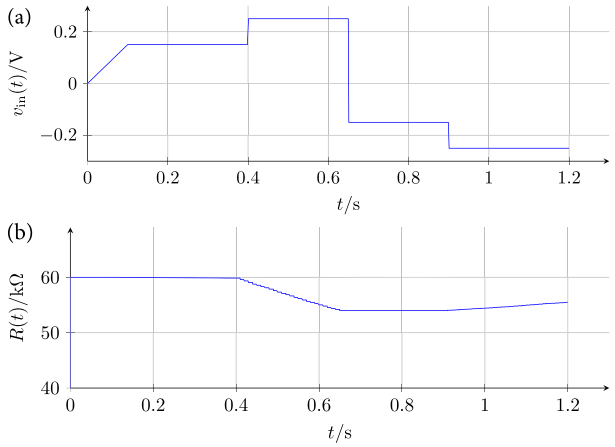

Figure 15. (a) Time waveform of a voltage signal v_{in} similar to the typical signal v_{int1} at the output of the first inverting integrator over a catch phase. (b) Memristance response to a pulse train-based stimulus shaped according to the voltage waveform in plot (a) (see text for details). [Colour figure can be viewed at wileyonlinelibrary.com]

strategy is a design parameter. It needs to be carefully chosen in such a way to allow a later memristance increase or decrease while keeping the device away from either saturation state, where the fully-on condition $R = R_{on}$ or fully-off condition $R = R_{off}$ applies, irrespective of the kick polarity. Further, the value for a resistance (specifically R_a in the circuit of Figure 17 to be described shortly) will have to be preliminarily selected through an offline optimisation procedure aimed at defining the perfect 'kick' for the motor-pendulum system. This is not a major disadvantage of the real nano-device-based control circuit implementation over the one adopting the ideal memristor (refer to Section 4), because in the latter case after the initialisation phase, the integration constant K_{int2}, or, equivalently, the resistance R_a in the circuit of Figure 4(d), has to be tuned via optimisation anyways.

However, the Knowm nano-device is well-suited to carry-out the adaptative integration of a pulse train stimulus shaped on the basis of the low-range voltage v_{int1} typically observed over the catch phase of successive KFC strategy runs. Let us gain further insights on the dynamics of the one-port under these conditions. One crucial feature of the Knowm memristor, which clearly differentiate it from the ideal memristor from Section 4, is its asymmetric dynamic behaviour. In other words, the device switching kinetics are strongly dependent upon the polarity of the voltage falling across its terminals. In the LTSpice simulation result in Figure 15, under a pulse train stimulus applied directly across the memristor terminals and shaped on the basis of the voltage waveform v_{in} shown in plot (a), the memristance of the one-port, with initial value 60 kΩ, evolves with time as shown in plot (b). The signal in plot (a) is similar to a typical voltage waveform at the output of the first inverting integrator during a catch phase. It has relatively short time intervals where it ascends or descends and relatively long time intervals where it is unchanged, as it happens during sense and drive phases, respectively. The pulse train-based stimulus applied across the memristor terminals is shaped in the following way. When the signal v_{in} in plot (a) is changing, the stimulus for the memristor is null. When the signal v_{in} in plot (a) is equal to a constant, a pulse train of period 10 ms and amplitude equal to the same constant over the first 500 ns and to 0 V over the remaining part of the period is applied across the device. The memristor acts as a resistor when the train pulse amplitude is set to ±150 mV. No change in the memristance function is appreciated in these scenarios (see plot (b)). However, under the larger train pulse amplitudes ±250 mV, the memristance undergoes evident changes, decreasing and increasing in an approximately linear fashion at higher and lower rate for the positive and negative polarity input, respectively. This asymmetric switching kinetics, typical in physical memristors [20], shall be taken into consideration in the shaping of the pulse train to be used to modulate the device memristance over a catch phase of the proposed KFC strategy under circuit implementation with the Knowm one-port.

As last test, in the LTSpice simulation result of Figure 16, the plot (b) shows the response of the device memristance, initiated once more from the value of 60 kΩ, under application of a pulse train

DOI: 10.1002/cta

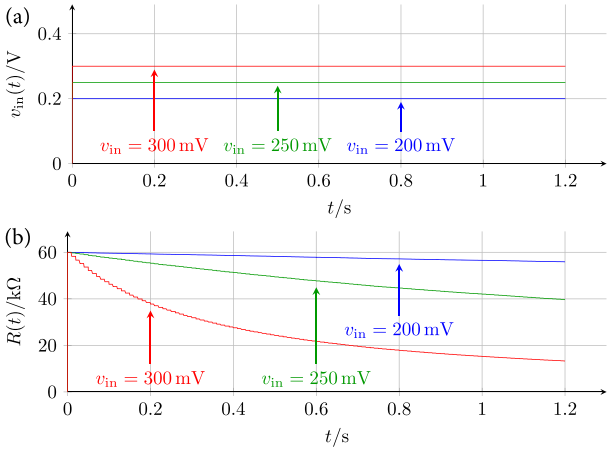

Figure 16. (a) Time evolution of a constant voltage signal v_{in} for three different DC values assigned to it. (b) Memristance over time in response to a pulse train stimulus shaped according to the voltage signal in plot (a) for each of its three values (see the text for details). [Colour figure can be viewed at wileyonlinelibrary.com]

shaped on the basis of each of the three positive constant levels in the voltage signal v_{in} illustrated in plot (a), specifically 200, 250 and 300 mV. In each case, the pulse train has a period of 10 ms and amplitude equal to the associated constant level in the signal of plot (a) over the first 500 ns of the period and to 0 V over the remaining part of the period. The best performance of the Knowm memristor as signal integrator is obviously achieved for the constant level of 200 mV.

A similar analysis was conducted under the case of negative constant levels in the signal v_{in}. The investigation revealed that an approximately linear response in the device memristance with similar rate as for the blue line in plot (b) of Figure 16 emerges under a pulse train amplitude of −250 mV.

On the basis of the results presented in this section, the memristance programming over a catch phase of the KFC strategy under circuit implementation with a Knowm device is carried out differently as compared with the approach reserved to the ideal memristor case (see Section 4). First, the initialisation phase is skipped here. The initial memristance of the device for the first application of the KFC strategy is a design parameter. Ideally, it should be chosen in such a way to allow subsequent memristance changes in both directions irrespective of the 'kick' polarity without driving the device into saturation. Further, the value for a resistance (particularly R_a in the circuit of Figure 17 to be presented in Section 5.2) will have to be determined beforehand through an offline optimisation procedure intended to obtain the best possible estimate for the first kick phase duration. Over each catch phase in the application of the proposed KFC strategy, provided the positive (negative) polarity voltage signal v_{int1} at the output of the first integrator exceeds the threshold of +(−)300 mV, the Knowm memristor is excited – starting from the beginning of a driving time interval – by means of a pulse train of period 10 ms (the sum of the time intervals $\Delta t_{sense} = 1$ ms and $\Delta t_{drive} = 9$ ms typically chosen for a sense phase and for a drive phase, respectively [12]) and amplitude equal to 200 mV (−250 mV) over the first 500 ns of the period and to 0 V over the remaining part of the period. The reason behind our choice to apply a non-null pulse across the Knowm memristor at the beginning of each drive phase only provided the modulus of the inverting integrator output voltage v_{int1} exceeds a threshold has to be researched in our attempt to preserve the device lifetime, which would be impaired quickly under continuous memristor pulse stimulation, which, however, is unnecessary when the pendulum undergoes small oscillations around the upright position, and the modulus of the voltage v_{int1} is consequently small.

5.2. Circuit-theoretic model for the estimate of the kick phase duration

Given the poor analogue signal integration performance of the Knowm memristor, discussed in Section 5.1, a novel strategy for the determination of a proper kick phase duration in the KFC control of a limb movement in Myon, other than the theoretical approach based upon the time integration of the analogue waveform corresponding to the first integrator output voltage v_{int1} throughout the previous catch phase, needs to be worked out. Here, we follow the empirical approach devised in Section 5.1,

DOI: 10.1002/cta

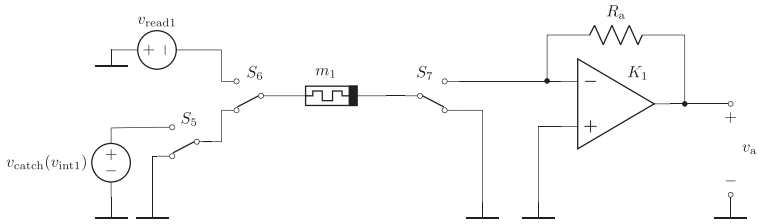

Figure 17. Core electronic system in the circuit implementation of the Kick-Fly-Catch control paradigm revolving around the use of the metastable switch memristor model of a real non-volatile memory cell fabricated at Knowm, Inc. The electronic system enables a v_{int1}-controlled pulse-based modulation of the nano-device memristance during the jth catch phase, its uncorrupted reading over the course of the following $(j+1)$th kick phase and its storage in the $(j+1)$th fly phase or whenever the robot is set in sleep mode (see text for details on the configurations of the switches for the three distinct operations of this circuit and note that $j \in \mathbb{N} = \{1, 2, 3, \ldots\}$). Note that v_a is not the voltage at the armature node A, which is referred to as v_{A} instead, as shown in Figure 1(a).

taking into consideration the fact that the typical technique adopted in the industry to modulate the conductance of real nanoscale memristors is based upon the application of pulse train-based stimuli.

Figure 17(a) illustrates the circuit allowing the programming of the Knowm memristor conductance carried out during the catch phase of the proposed KFC strategy through the application of an appropriate pulse train, shaped on the basis the first integrator output voltage v_{int1} as described at the end of the previous section. Over the sense phase and over most of the time of a drive phase – specifically throughout the catch phase except, under a specific condition (see subsequent discussion), the first time interval Δt_{prog} of a drive phase, the switches S_5, S_6 and S_7 are clicked into their lower positions, resulting in a zero voltage falling across the memristor. During the first time interval Δt_{prog} of a drive phase, instead, the switch S_5 assumes the complementary position, coupling the voltage-controlled voltage source $v_{\mathrm{catch}}(v_{\mathrm{int1}})$ to the grounded memristor, thus allowing its excitation with a pulse of amplitude $V_{\mathrm{catch,pos}}$ ($V_{\mathrm{catch,neg}}$) under a positive (negative) polarity first integrator output voltage v_{int1}, provided the modulus of the latter signal exceeds a specific threshold $V_{\mathrm{catch,th}}$.

Recalling that the catch phase of the jth KFC strategy run spans the time interval $[t_{0,\mathrm{c}}^{(j)}\ t_{\mathrm{f,c}}^{(j)})$, the memristance of the nanodevice at $t = t_{\mathrm{f,c}}^{(j)}$, i.e. $R(t_{\mathrm{f,c}}^{(j)})$, depends upon its value at $t = t_{0,\mathrm{c}}^{(j)}$, i.e. $R(t_{0,\mathrm{c}}^{(j)})$, unaltered during the previous jth kick and fly phases with respect to its value at the beginning of the jth KFC strategy run, and upon its response to a pulse train-based signal $v_{\mathrm{catch}}(v_{\mathrm{int1}})$ shaped on the basis of the time waveform of the first integrator output voltage v_{int1} during the jth programming phase (here, $j \in \mathbb{N} = \{1, 2, 3, \ldots\}$).

The same circuit in Figure 17(a) permits to carry out a non-disruptive reading of the Knowm device resistance over the course of the following $(j+1)$th kick phase,[‡‡] if switches S_6 and S_7 are set to the complementary configurations with respect to the ones visualised in the plot, while S_5 assumes the lower position. The memristance is read through the computation of the circuit output voltage v_a, which, throughout the $(j+1)$th kick phase, is found to be given by the following DC value:

$$v_{\mathrm{a}} = \frac{R_{\mathrm{a}}}{R(t_{\mathrm{f,c}}^{(j)})}\, v_{\mathrm{read1}}. \tag{56}$$

All in all, the circuit of Figure 17 plays here the same role as the circuitry in Figures 4(a)–(d) for the KFC strategy circuit implementation revolving around the use of the ideal memristor emulator.

The Knowm-based and emulator-based KFC control circuit implementations share the use of the circuit of Figure 4(d) to estimate the time $t_{0,\mathrm{f}}^{(j+1)} \equiv t_{\mathrm{f,k}}^{(j+1)}$ at which the $(j+1)$th fly phase should commence.

[‡‡]In principle, the reading operation could be performed just once at the end of the jth catch phase. However, the circuit implementation is simpler when the measurement of $R(t_{\mathrm{f,c}}^{(j)})$ goes on throughout the $(j+1)$th kick phase. Because the real memristor from Knowm, Inc. [16] is practically insensitive to very low voltage stimuli, by choosing an appropriate value for the sensing voltage signal v_{read1}, the continuous reading operation over the $(j+1)$th kick phase does not corrupt the device resistance (see later for details).

DOI: 10.1002/cta

Recalling that the initial time of the $(j+1)$th KFC paradigm application, i.e. $t_{\mathrm{i}}^{(j+1)} = t_{0,\mathrm{k}}^{(j+1)}$ is set to 0 s, the output voltage v_{out} in the circuit of Figure 4(d) evolves over time according to Equation 37, derived analytically in Section 4. Using the analytical formula for v_{a} from Equation 56 into Equation 37, an estimate for the time span of the $(j+1)$th kick phase is obtained by setting v_{out} to 0 V, leading to

$$\begin{aligned} t_{\mathrm{f,k}}^{(j+1)} &= \frac{v_{\mathrm{a}}}{K_{\mathrm{ctrl}} \cdot v_{+}} \\ &= \frac{R_{\mathrm{a}}}{R(t_{\mathrm{f,c}}^{(j)})} v_{\mathrm{read1}} \cdot \frac{1}{K_{\mathrm{ctrl}} \cdot v_{+}}, \end{aligned} \tag{57}$$

where K_{ctrl} is defined as in Section 4.

Remark 4
Similarly as the ideal memristor emulator, the Knowm memristor's resistance decreases (increases) under negative stimuli. It follows that, in case the jth 'kick' delivered to the dynamic system were too weak (strong), resulting in a positive (negative) time waveform of the voltage v_{int1} at the output of the first inverting integrator during the catch phase, the positive (negative) pulses in the programming train exciting the nano-device throughout this phase shall induce a memristance decrease (increase), with the consequent reduction (growth) of $R(t_{\mathrm{f,c}}^{(j)})$ with respect to $R(t_{0,\mathrm{c}}^{(j)})$, and the resulting shrinking (stretching) in the time span of the $t_{\mathrm{f,k}}^{(j+1)}$ kick phase according to Equation 57.

When $v_{\mathrm{out}}(t)$ in the circuit of Figure 4(d) attains the null value, the three switches in Figure 17 are configured in the shown configuration to allow a safe storage of the memristor resistance in the $(j+1)$th fly phase (the nonvolatile memory capability of the memristor is also harnessed when the power to the Myon is switched off in the sleep mode). Meanwhile, the circuit of Figure 5 monitors the armature voltage v_{A} to detect the end of the $(j+1)$th fly phase. When this occurs a new $(j+1)$th catch phase may begin. At $t = t_{\mathrm{i}}^{(j+1)} \equiv t_{0,\mathrm{c}}^{(j+1)}$, the voltage v_{int1} at the output of the first integrator restarts from 0 V, while the memristance initial value is given by $R(t_{0,\mathrm{c}}^{(j+1)}) = R(t_{\mathrm{f,c}}^{(j)})$.

Despite, unlike the ideal emulator, the Knowm memristor-based control circuit is unable to carry out a proper time integration of the voltage signal v_{int1} over the jth catch phase, the circuit in Figure 4(d) derives an accurate estimate for the $(j+1)$th kick phase time span on the basis of a pulse-based memristance modulation controlled by polarity and modulus of the first integrator output voltage v_{int1}, accomplished throughout the previous jth catch phase by means of the empirical study-based circuit of Figure 17 with S_5 clicked in the upper configuration.

5.3. Time efficiency, energy savings and adaptation of the Knowm memristor-based control circuit

The circuit model of the motor-pendulum system under KFC control with a Knowm memristor is thus the collection of circuits shown in Figures 3, 4(e), 5 and 17 (where the memristor was modelled as a subcircuit implementing the MSS model revisited in Section 3.2). Except for the circuit of Figure 17 and for the memristor model, the Knowm device-based and the ideal memristor-centered KFC strategy circuit implementations share the same circuitry.

The circuit parameters for the circuit of Figure 3 are given in Table I of the companion part I paper [12], except for the maximum control voltage applied to the armature node A during a kick phase, which is set as specified in Equation 48.

In each application of the control strategy, the initial conditions for the circuit variables i_{A}, v_{int1}, i_1, v_{C} and $v_{\mathrm{C_{sah}}}$, respectively, associated to dynamic one-ports [24] L_{A}, C_1, L_1, C_{pos} and C_{sah} in the circuits of Figures 3(b–e) and 5(b) are set as in the circuit implementation of the KFC strategy revolving around the use of the ideal memristor emulator. Unlike the circuit implementation discussed in Section 4, here, we do not strictly compute the time integral of the voltage v_{int1} over a catch phase. This notwithstanding, before the first application of the KFC strategy, the choice of a suitable initial condition for the memristive dynamic element, which allows to estimate the duration of the next kick phase through a v_{int1}-controlled pulse-based modulation of its memristance over the previous catch phase, is instrumental for the correct functioning of the control system. Throughout the simulations to follow, the Knowm

DOI: 10.1002/cta

Table V. Parameter values for the circuit of Figure 17. The threshold voltage $V_{\text{catch,th}}$ for memristance programming over a catch phase was chosen so as to limit the degradation in the Knowm memristor endurance while keeping the error in the estimate of the next kick phase duration as low as possible.

Parameter	Value	Parameter	Value
v_{read1}	125 mV	$V_{\text{catch,neg}}$	−250 mV
$V_{\text{catch,pos}}$	200 mV	R_{a}	346.95 kΩ
$V_{\text{catch,th}}$	300 mV	Δt_{prog}	500 ns

device memristance is initially set to $R(t_{\text{i}}^{(1)}) = R(t_{0,\text{k}}^{(1)}) = 51.34\,\text{k}\Omega$. The initial condition on the memristance for the first application of the KFC strategy is a design parameter. It was chosen well within the allowable range[§§] $[R_{\text{on}}, R_{\text{off}}] = [333\,\Omega, 1\,M\Omega]$ so that the memristance would not saturate to either bound at the end of each adaptive catch phase.

Table V tabulates the circuit parameter values for the circuit of Figure 17. It is important to observe that the chosen value for v_{read1} leads to a perfectly uncorrupted memristance read throughout a kick phase, because the Knowm device does not respond at all to small DC voltage stimuli of this kind. Furthermore, as mentioned previously, the value for the resistance R_{a} was optimised offline before the first application of the KFC paradigm to obtain the best possible 1st kick phase duration estimate, while making sure its value was not falling well below, the MΩ range to keep the power dissipation as low as possible in the circuit of Figure 17 over the memristance reading process (i.e. over the kick phase) and taking into account the aforementioned value for the memristance at the beginning of the first application of the KFC control strategy.

Finally, the circuit parameters for the circuits in Figures 4(e) and 5 are reported in the last two rows of Tables II and III, respectively.

Figure 18 shows LTSpice simulation results on the circuit-theoretic model of the overall dynamic system under the first application of the Knowm memristor-centred KFC control strategy to an inverted pendulum with a rod of length $l = 10\,\text{cm}$ and load mass $m = 10\,\text{g}$. Plots (a–e), respectively, illustrate the time evolution of the control voltage v_{ctrl}, of the first integrator output voltage v_{int1}, of the Knowm memristor resistance $R(t)$, of the pendulum angle γ and of the cost function $C(t)$. In all plots, the kick, fly and catch phases are clearly marked. Specifically, the kick and fly phase time intervals, respectively, are $[t_{0,\text{k}}^{(1)}, t_{\text{f,k}}^{(1)}) = [0, 0.835)\,\text{s}$ and $[t_{0,\text{f}}^{(1)}, t_{\text{f,f}}^{(1)}) = [0.835, 1.26)\,\text{s}$. Further, the initial time of the catch phase is $t_{0,\text{c}}^{(1)} = 1.26\,\text{s}$. The final simulation time is set to 4.5 s. Very importantly, the performance levels attained by the KFC strategy circuit implementation revolving around the use of the Knowm memristor in terms of time-efficiency and energy-efficiency are similar to the corresponding ones featured by the ideal emulator-centred circuit-theoretic model of the proposed control approach. The 'kick' delivered to the motor-pendulum system – refer to plot (a) is already fairly good, lifting the pendulum very close to the target position. In the fly phase, the rod passes slightly over the upright position, and the pendulum angle – see plot (d) – goes only slightly negative, as demonstrated by the tiny negative dip in the time waveform of the first integrator output voltage – look at plot (b) – before increasing towards the target position and oscillating around it during the catch phase. The Knowm memristor resistance undergoes no changes in this phase, demonstrating the appropriateness of the 'kick' delivered to the system. The time needed to lift the pendulum from the position identified by the angle $\gamma(t_{0,\text{k}}^{(1)}) = 3.04$ to the location defined by the threshold angle $\gamma_{\text{th}} = 0.1$ is found to be equal to

$$\Delta t = t|_{\gamma=\gamma_{\text{th}}} - t|_{\gamma=\gamma(t_{\text{i}})} = 1.02s, \tag{58}$$

[§§] Choosing a value for $R(t_{\text{i}}^{(1)}$ around the middle of the memristance range, i.e. 500 kΩ, would have led to an unreasonably huge value for R_{a}.

DOI: 10.1002/cta

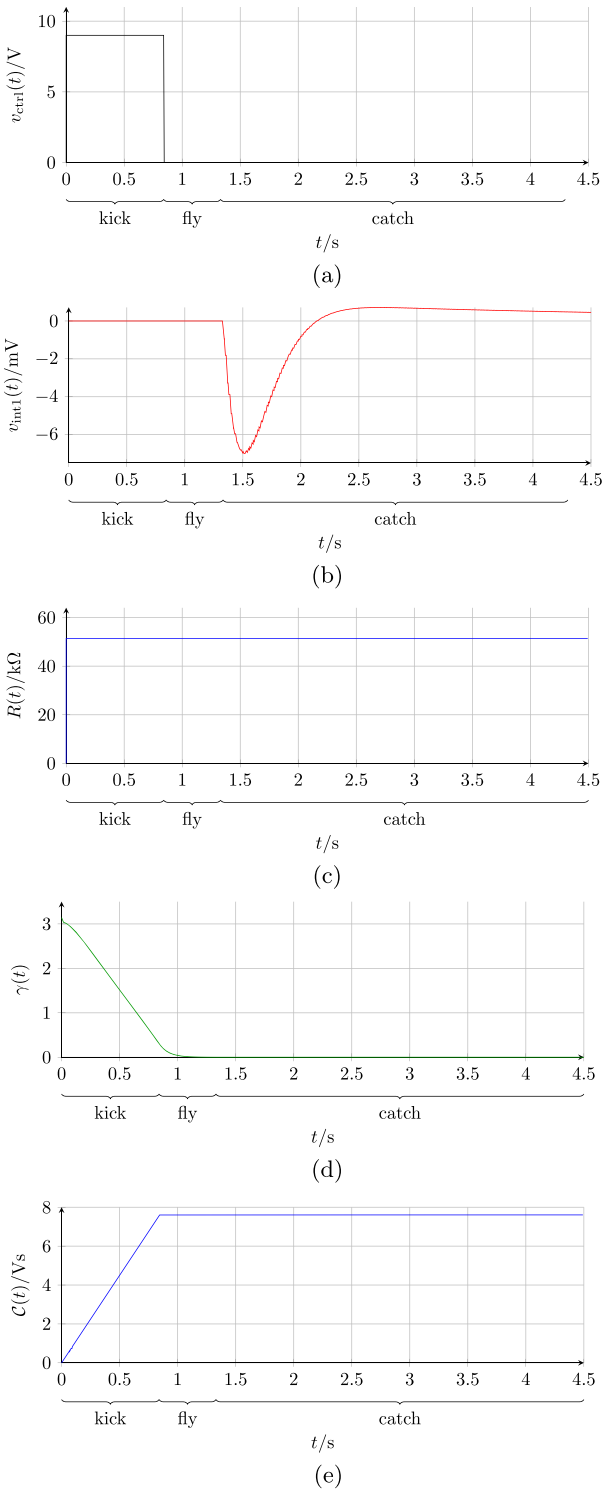

Figure 18. Time evolution of control voltage (a), first integrator output voltage (b), Knowm nano-device memristance (c), pendulum angle (d) and cost function (e) under the first application of the proposed Kick-Fly-Catch paradigm to the motor-pendulum system for a rod with length $l = 10\,\mathrm{cm}$ and a load mass $m = 10\,\mathrm{g}$ from a LTSpice simulation of the circuitry of Figures 3, 4(e), 5 and 17 (where the memristor was modeled as a subcircuit implementing the metastable switch model revisited in Section 3.2). [Colour figure can be viewed at wileyonlinelibrary.com]

DOI: 10.1002/cta

which is very close to the equivalent measurement carried out on the emulator-based KFC strategy circuit implementation and, most importantly, is way shorter than the corresponding time of 17.8 s recorded in the LTSpice simulation on the circuit-theoretic model of the GAF control paradigm [12].

The measurement of the cost function, evaluated at the time $t|_{\gamma=\gamma_{\text{th}}}$ at which the pendulum attains the position defined by the threshold angle, is

$$C(t|_{\gamma=\gamma_{\text{th}}}) = 7.42\ Vs, \tag{59}$$

which is not far from the equivalent calculation carried out on the emulator-based KFC strategy circuit implementation and, most crucially, is much lower than the corresponding cost of 20.4 Vs evaluated in the LTSpice simulation on the circuit-theoretic model of the GAF control paradigm [12].

The Knowm memristor-based circuit-theoretic model has a weaker adaptability to changes in the pendulum topology and to perturbations to the dynamic system initial conditions as compared with the circuit realisation revolving around the use of the ideal memristor emulator. This is because of the well-known extreme sensitivity of the response of real memristor nano-devices to tiny changes in their stimuli [20]. This notwithstanding, the following tests show that the circuit implementation of the KFC control strategy with the Knowm nano-device may tune its operation to achieve a faster pendulum lift under a lower energy budget expenditure as the pendulum load mass is changed after the derivation of the optimal value for the resistance R_{a} (refer to the circuit of Figure 17) in the nominal case, where m was equal to 10 g.

Plots (a) and (b) in Figure 19, respectively, show the pendulum angle and the nano-device memristance over time observed in a LTSpice simulation of the circuits of Figures 3, 4(e), 5 and 17 (a subcircuit, implementing the mathematical description of the Knowm nano-device from Section 3.2, was used to model the memristor in the latter circuit) for three distinct scenarios, where the pendulum load mass m is set to values falling in the set {15, 20, 25} g after the optimisation of the resistance R_{a} from Figure 17, previously tuned to the nominal load mass value of 10 g. As may be evinced from plot (a), in each case, the first 'kick' delivered to the motor-pendulum system is too short, given the non-negligible distance of the rod from the target position at the beginning of the fly phase. The resulting

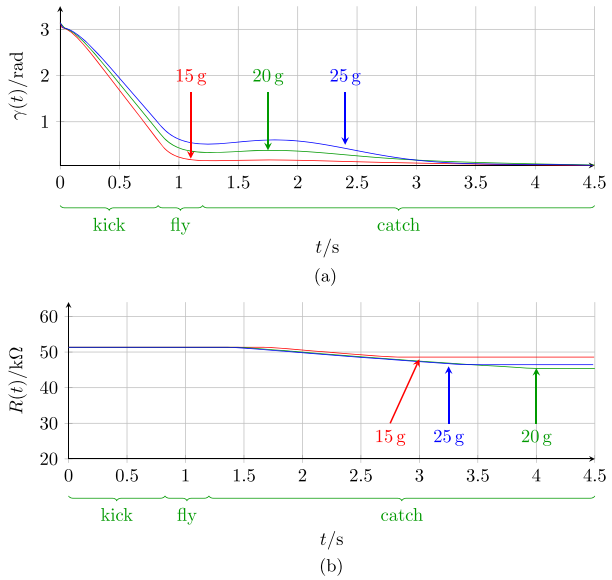

Figure 19. LTSpice simulation results on the Knowm memristor-centred circuit-theoretic model of the motor-pendulum system under Kick-Fly-Catch control strategy. Time evolution of pendulum angle γ (a) and of nano-device memristance R (b) in the first strategy run for the case of load masses larger than the nominal value of 10 g. The initial conditions for the physical quantities shown in plots (a) and (b) are 3.04 and 51.34 kΩ, respectively. The three phases are clearly marked for the scenario corresponding to the choice $m = 20$ g. [Colour figure can be viewed at wileyonlinelibrary.com]

DOI: 10.1002/cta

decrease in the nano-device memristance over the adaptive catch phase allows to stretch the duration of the kick phase in the second application of the KFC strategy.

Unfortunately, unlike what occurred in the emulator-centred circuit implementation of the paradigm, here, the decrease in the value of the device memristance at the end of the first catch phase is non-monotonous as the pendulum load mass increases. It follows that, here, in general, the resulting 'kick' calibration may be not as good as in the case of the ideal memristor-based circuit model from Section 4. In fact, as demonstrated in Figure 20(a), the new 'kick' is better than the old one but still too short for the largest mass $m = 25\,\mathrm{g}$, where at the beginning of the fly phase, the rod has not yet attained the upright position, whereas it is too long for the remaining two masses of 15 and 20 g, which travel over

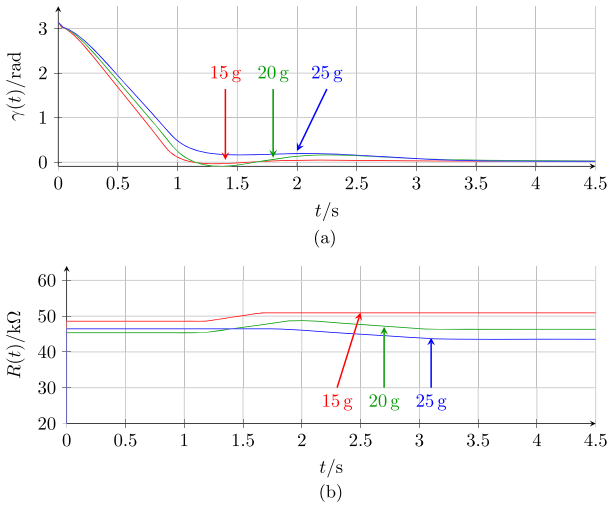

Figure 20. LTSpice simulation results on the circuitry in Figures 3, 4(e), 5 and 17 (in the latter circuit the Knowm memristor is defined as a subcircuit implementing the mathematical model revisited in Section 3.2). Pendulum angle γ (a) and Knowm memristor resistance R over time in the second strategy application for load masses in the set $\{15, 20, 25\}$ g. In each load mass scenario, the initial condition for the memristance is set to the last value it attained in the first catch phase. [Colour figure can be viewed at wileyonlinelibrary.com]

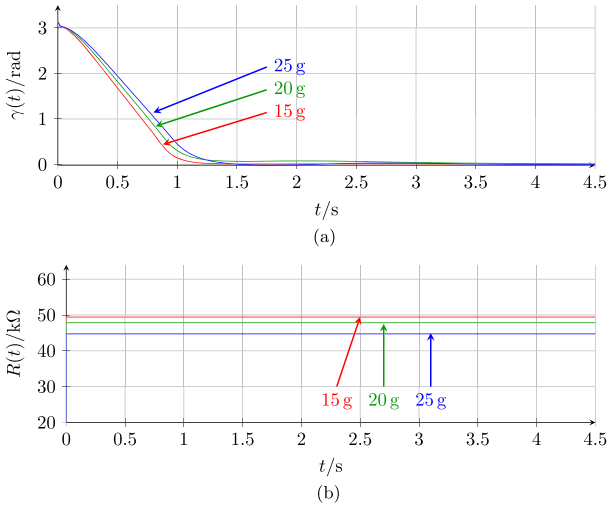

Figure 21. LTSpice simulation of the Knowm memristor-based circuit implementation of the motor-pendulum under Kick-Fly-Catch control. Time waveform of the pendulum angle (a) and of the nano-device memristance (b) in the nth strategy run for the case of larger load masses than the nominal value of 10 g. Here, n is numerically equal to four for $m = \{15, 25\}$g, and to seven for the mass of 20 g. In each load mass scenario, the initial condition for the memristance is set to the last value it attained in the $(n-1)$th catch phase. [Colour figure can be viewed at wileyonlinelibrary.com]

DOI: 10.1002/cta

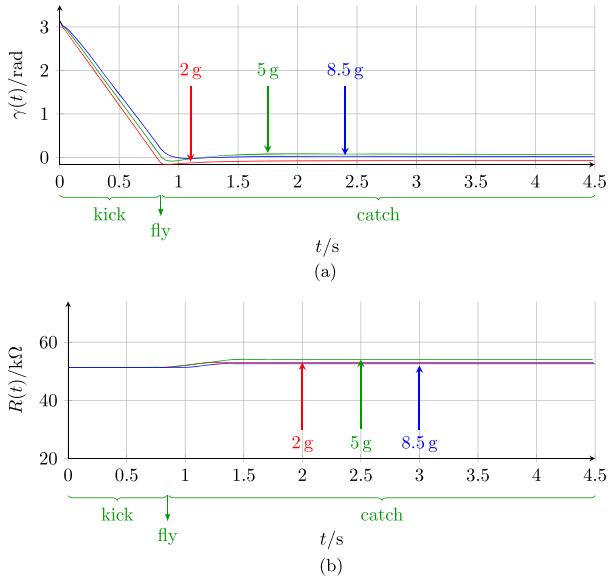

Figure 22. LTSpice simulation results on the Knowm memristor-centred circuit-theoretic model of the motor-pendulum system under Kick-Fly-Catch control strategy. Time evolution of pendulum angle γ (a) and of nano-device memristance R (b) in the first strategy run for the case of load masses smaller than the nominal value of 10 g. The initial conditions for the physical quantities shown in plots (a) and (b) are 3.04 and 51.34 kΩ, respectively. The three phases are clearly marked for the scenario corresponding to the choice $m = 5$ g. Despite it is not well visible, there emerges a small negative overshoot in the time waveform of γ over the kick phase also for the load mass of 8.5 g. [Colour figure can be viewed at wileyonlinelibrary.com]

the target state descending from the other side of the x axis (refer to Figure 1(b)) – down to a position with lower height for the higher load mass – during the second fly phase. It follows that for $m = 25$ g, the Knowm memristor resistance undergoes yet another decrease over the second catch phase, leading to a further lengthening of the next kick phase time span, while for the other two masses of 15 and 20 g, the memristance is coincidentally subject to a net increase[¶¶], prompting a shortening of the 'kick' for a later application of the KFC strategy (refer to plot (b) in Figure 20). After a few applications of the KFC paradigm, particularly four for $m = \{15, 25\}$ g and seven for $m = 20$ g, the 'kick' given to the inverted pendulum is optimal. The pendulum is lifted speedily in the neighbourhood of the target position – see plot (a) in Figure 21 – and no noticeable device memristance change is observed during the catch phase.

Because, unlike the ideal emulator, the Knowm memristor features different switching dynamics for stimuli of distinct polarity and fixed modulus, it is of interest to study the response of the nano-device-based KFC strategy circuit implementation for the case where the load mass m is decreased with respect to the original nominal value of 10 g after the resistance R_a in the circuit of Figure 17 is optimised for the nominal mass value. In all three cases, where the load mass assumes values in the set $\{2, 5, 8.5\}$ g, the first application of the KFC paradigm results in a negative overshoot during the first kick phase – see plot (a) in Figure 22 – leading to an increase in the device memristance over the catch phase – see plot (b) in Figure 22 – which finally result in a shrinking of the time period for the application of the maximum control voltage at the armature node in the second strategy run.

Figure 23 shows the LTSpice simulation results on the Knowm device-based circuit implementation of the proposed KFC control methodology under the second strategy application to the motor-pendulum system with rod load masses larger than the nominal value of 10 g for which the resistance R_a in the circuit of Figure 17 was originally optimised. The second 'kick' delivered to the system is already very good for the masses in the set $\{5, 8.5\}$ g, as clear from plot (a) in Figure 23. No sign of corruption in

[¶¶]For the larger of these two load masses, the memristance first undergoes an increase but then is subject to a less significant decrease, because of the non-negligible positive hill in the time waveform of the pendulum angle following the climb back up from the negative overshoot.

DOI: 10.1002/cta

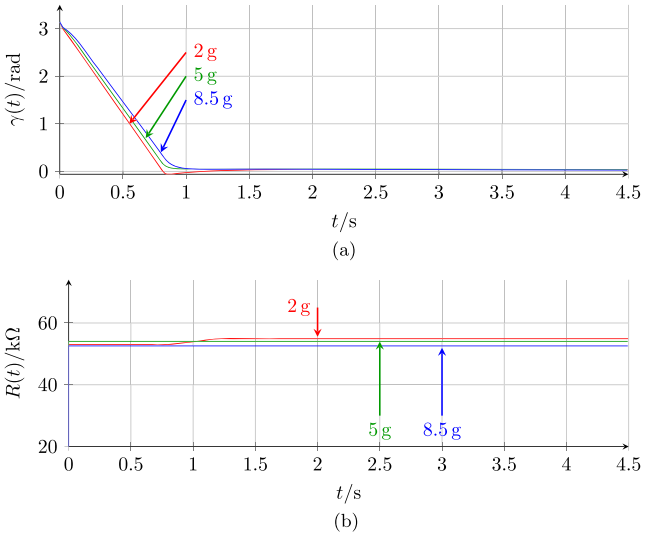

Figure 23. LTSpice simulation results on the circuitry in Figures 3, 4(e), 5 and 17 (in the latter circuit the Knowm memristor is defined as a subcircuit implementing the mathematical model revisited in Section 3.2). Pendulum angle γ (a) and Knowm memristor resistance R over time in the second strategy application for load masses in the set $\{2, 5, 8.5\}$ g. In each load mass scenario, the initial condition for the memristance is set to the last value it attained in the first catch phase. [Colour figure can be viewed at wileyonlinelibrary.com]

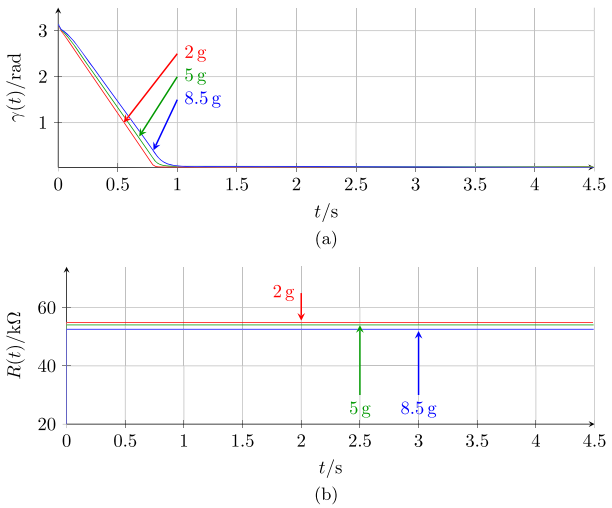

Figure 24. LTSpice simulation of the Knowm memristor-based circuit implementation of the motor-pendulum under Kick-Fly-Catch control. Time waveform of the pendulum angle (a) and of the nano-device memristance (b) in the third strategy run for the case of smaller load masses than the nominal value of 10 g. In each load mass scenario, the initial condition for the memristance is set to the last value it attained in the second catch phase. [Colour figure can be viewed at wileyonlinelibrary.com]

the device resistance is appreciated over the catch phase for these two scenarios (refer to plot (b) in Figure 23). With regard to the scenario pertaining to the smaller load mass of 2 g, the second 'kick' leads to a faster pendulum lift than the first one but still results into a small negative overshoot before the beginning of the second fly phase (see plot (a) in Figure 23). Consequently, here, the memristance undergoes a little growth over the catch phase (refer to plot (b) in Figure 23), leading to a reduction in the time span of a successive kick phase.

In the third application of the KFC paradigm for all load mass cases, the pendulum attains a position in the neighbourhood of the unstable upright state in a very short time (see plot(a) in Figure 24), and

DOI: 10.1002/cta

we witness a constant time behaviour of the device memristance over the catch phase (refer to plot (b) in Figure 24), certifying the accuracy of the current kick phase duration.

Summarising the main research findings unveiled in this section, our investigations have revealed the feasibility to implement the KFC paradigm by means of a circuit employing a real memristor from Knowm Inc. [16], although some issues need to be addressed to ensure a smooth run of the proposed control approach. The device does not perform an ideal analog integration. Because of its highly-nonlinear and stochastic dynamic behaviour, the Knowm memristor is unable to integrate signals characterised by a large dynamic range, such as the typical waveform at the output of the inverting integrator during the run of an initialisation phase. It follows that, here, such preliminary GAF strategy application is not contemplated. Rather, after the selection of a suitable initial device memristance, an optimisation procedure is carried out offline before the first application of the KFC strategy to determine the most appropriate resistance value for the resistor R_a in the circuit of Figure 17 with the aim to define the most appropriate first 'kick' to deliver to the motor-pendulum system. Importantly, under pulse-based stimuli of limited amplitude, the Knowm device memristance responds in an approximately-linear fashion, and this integrating behaviour was harnessed in the derivation of a new memristance programming technique for the 'kick'-correcting catch phases. An advantage of the Knowm device over the ideal emulator lies in its insensitivity to stimuli below a certain threshold, which guarantees an uncorrupted memristance reading over a kick phase and a reduced power-consumption during the memristance modulation throughout a catch phase.

Remark 5

As a very final remark, in the case of negative 'kicks,' the circuit in Figure 17 may still be used in combination with the circuit of Figure 4(d) to estimate the kick phase duration in the next application of the proposed KFC strategy provided the memristor polarity in the first circuit is reversed. In fact, under this condition, a negative (positive) inverting integrator output voltage over a catch phase, calling for a longer (shorter) kick in the next KFC strategy run, would lead to a coincidental reduction (growth) in the device memristance via pulse-based modulation from its initial value (which may be kept equal to 51.34 KΩ), as desired, given the inverse proportionality between the next kick phase time span and the device memristance at the end of the past catch phase (see Equation 57). Of course, other alternative circuit designs are possible under negative 'kicks', i.e. the one proposed here is only one simple solution.

6. CONCLUSIONS AND FUTURE RESEARCH DEVELOPMENTS

Neuromorphic circuits shall be considered in future electronic systems for energy-efficient computing based on biological principles. In bio-inspired artificial neural networks, memristors [25–29] are used as neuron and/or synapse models in several recent investigations [30] in order to overcome the limits of conventional von Neumann architectures by adopting these devices as memory elements and as computing units. Cellular neural networks [31, 32], high-speed dynamic processor arrays with stored programmability for universal computation (e.g. multivariate signal processing, pattern recognition and biological system modeling), are already based on the principle of distributed memcomputing.

A first approach to the principle of combined sensing [33–35] and computing [36, 37] was presented in this two-part contribution. The standard GAF methodology [2] for limb movement control in the humanoid robot Myon [38] leads to stable behaviour, but the resulting motion is slow and consumes a lot of energy. The part I paper [12] first discussed the downsides of the original GAF strategy and then introduced the system-theoretic foundations of a novel bio-inspired motion control paradigm, called 'KFC', in which the principle of mem-computing lies at the basis of fast and energy-efficient robot limb movements, thus enhancing considerably the performance achieved with the standard approach while maintaining its topology-adaptive nature.

In this part II manuscript, a circuit theoretic model for the motor-pendulum system under the innovative memristor-centred KFC CSL control strategy was first presented. Employing the model [14] of an ideal memristor [5] for the mathematical description of the key element in the novel control electronic system, we demonstrated the accuracy of the theory developed in the part I paper [12] through a number of LTSpice simulations of the circuitry of the overall dynamic system. The tests revealed the considerable enhancement in performance of the proposed control system over the state-of-the-art

DOI: 10.1002/cta

GAF circuitry, which is currently implemented in the CSL of each joint of Myon, in terms of time-efficiency and energy-efficiency. Subsequently, we also validated the novel control strategy employing the model of a real nanodevice from Knowm, Inc. [16] to characterise the memcomputing element in the control circuitry. Because of the poor performance of physical memristor devices as integrators[‖‖], the circuit implementation of the control system was modified so as to estimate the time duration of a kick phase by applying a pulse-based memristance programming methodology in place for the analog input-driven conductance modulation scheme adopted for the ideal memristor-based feedback circuit. Apart from a weaker adaptability to changes in the external environment, due to the high sensitivity of a real memristor device to tiny changes in its stimulus, the Knowm memristor-based KFC control circuit attains similar performance levels as the ideal memristor-centred counterpart, justifying our future goal to fabricate a KFC CSL control electronic system and embed it in each joint of Myon.

ACKNOWLEDGMENTS

The support from EU COST Action IC1401 is acknowledged. We also thank the Deutsche Forschung Gesellschaft (DFG) for their financial contribution to the research project 'Locally active memristive data processing (LAMP)' (Grant Number TE 257/22-1). L. O. Chua's research is supported by AFOSR (Grant Number FA 9550-13-1-0136).

REFERENCES

1. Hild M, Siedel T, Benckendorff C, Thiele C, Spranger M. Myon, a new humanoid. In *Language Grounding in Robots*, Steels L, Hild M (eds). Springer: New York, 2012; 25–44.
2. Hild M. Defying Gravity - A Minimal Cognitive Sensorimotor Loop Which Makes Robots With Arbitrary Morphologies Stand Up. *11th International Conference on Accomplishments in Electrical and Mechanical Engineering and Information Technology (DEMI)*, Banja Luka, Bosnia and Herzegovina, 2013; 23–34.
3. Hild M, Kubisch M. Self-exploration of autonomous robots using attractor-based behavior control and ABC-learning. *11th Scandinavian Conference on Artificial Intelligence (SCAI)*, Trondheim, Norway, 2011; (10pp).
4. Hild M. Roboter mit robustem Verhalten. *Bulletin* 2013; **10s**:12–15.
5. Chua LO. Memristor - The missing circuit element. *IEEE Transaction on Circuit Theory* 1971; **18**(5):507–519.
6. Chua LO. Resistance switching memories are memristors. *Applied Physics A* 2011; **102**:765–783.
7. Biolek Z, Biolek D, Biolkova V. Computation of the area of memristor pinched hysteresis loop. *IEEE Transactions on Circuits and Systems II: Express Briefs* 2012; **59**(9):607–611. https://doi.org/10.1109/TCSII.2012.2208670.
8. Biolek D, Biolek Z, Biolkova V, Kolka Z. Some fingerprints of ideal memristors. *IEEE Int. Symp. Circuits and Systems (ISCAS)*, 2013; 201–204. https://doi.org/10.1109/ISCAS.2013.6571817.
9. Chua LO. If it's pinched, It's a memristor. *Special Issue on Memristive Devices, Semiconductor Science and Technology* 2014; **29**(10):104001 (42pp).
10. Chua LO. Everything you wish to know about memristors but are afraid to ask. *RadioEngineering* 2015; **24**(2): 319–368. https://doi.org/10.13164/re.2015.0319.
11. Pontryagin LS. *The Mathematical Theory of Optimal Processes, Classics of Soviet Mathematics*. Gordon and Breach Science Publishers S.A.: Montreux; Switzerland, 1986. ISBN-13: 978-2881240775.
12. Ascoli A, Baumann D, Tetzlaff R, Chua LO, Hild M. Memristor-enhanced humanoid robot control system–Part I: theory behind the novel memcomputing paradigm. *International Journal of Circuit Theory and Applications (IJCTA)* 2017. https://doi.org/10.1002/cta.2431.
13. Linear Technology. *LTspice IV Getting Started Guide*, 2011. url:http://cds.linear.com/docs/en/software-and-simulation/LTspiceGettingStartedGuide.pdf.
14. Kim H, Sah MPd, Yang C, Cho S, Chua LO. Memristor emulator for memristor circuit applications. *IEEE Transactions on Circuits and Systems - I: Regular Papers* 2012; **59**(10):2422–2431.
15. Molter TW, Nugent A. *The generalized metastable switch memristor model*. Dresden: Germany, 2016.
16. http://knowm.org.
17. Strukov DB, Snider GS, Stewart DR, Williams RS. The missing memristor found. *Nature* 2008; **453**:80–83.
18. Pan F, Gao S, Chen C, Song C, Zeng F. Recent progress in resistive random access memories: Materials, switching mechanisms, and performance. *Materials Science and Engineering: R: Reports* 2014; **83**:1–59.

[‖‖] In view of the considerable efforts spent nowadays to reengineer materials in order to achieve desired features in manufactured devices, with the expected progress in memristor fabrication process over the years to come, we envision that the availability of nanostructures acting as ideal integrators on the integrated circuit market will become reality sooner or later.

DOI: 10.1002/cta

19. Corinto F, Ascoli A, Gilli M. Analysis of current-voltage characteristics for memristive elements in pattern recognition systems. *International Journal of Circuit Theory and Applications* 2012; **40**(12):1277–1320. https://doi.org/10.1002/cta.1804.
20. Ascoli A, Tetzlaff R, Chua LO, Strachan JP, Williams RS. History erase effect in a non-volatile memristor. *IEEE Transactions on Circuits and Systems I: Regular Papers* 2016; **63**(3):389–400. https://doi.org/10.1109/TCSI.2016.2525043.
21. Corinto F, Forti M. Memristor circuits: Pulse programming via invariant manifolds. *IEEE Transactions on Circuits and Systems I: Regular Papers* 2017. https://doi.org/10.1109/TCSI.2017.2740999.
22. Slesazeck S, Mähne H, Wylezich H, Wachowiak A, Radhakrishnan J, Ascoli A, Tetzlaff R, Mikolajick T. Physical model of threshold switching in NbO2 based memristors. *RSC Advances* 2015; **124**(5):102318–102322. https://doi.org/10.1039/C5RA19300A.
23. Ascoli A, Ntinas V, Tetzlaff R, Sirakoulis GCh. Closed-form analytical solution for on-switching dynamics in a TaO memristor. *IEEE IET Electronics Letters* 2017; **53**(16):1125-1126. https://doi.org/10.1049/el.2017.1622.
24. Chua LO, Desoer CA, Kuh EA. *Linear and Nonlinear Circuits*. McGraw Hill: New York, 1985.
25. Corinto F, Ascoli A, Gilli M. Nonlinear dynamics of memristor oscillators. *IEEE Transactions Circuits and Systems–I* 2011; **58**(6):1323–1336. https://doi.org/10.1109/TCSI.2010.2097731.
26. Ascoli A, Slesazeck S, Mähne H, Tetzlaff R, Mikolajick T. Nonlinear dynamics of a locally-active memristor. *IEEE Transactions on Circuits and Systems I: Regular Papers* 2015; **62**(4):1165–1175. https://doi.org/10.1109/TCSI.2015.2413152.
27. Corinto F, Chua LO, Civalleri PP. A theoretical approach to memristor devices. *IEEE Journal on Emerging and Selected Topics in Circuits and Systems* 2015; **5**(2):123–132. https://doi.org/10.1109/JETCAS.2015.2426494.
28. Ascoli A, Tetzlaff R, Chua LO, Yi W, Williams RS. Memristor emulators: A note on modeling. In *Advances in Memristors, Memristive Devices and Systems, Studies in Computational Intelligence 701*, Vaidyanathan S, Volos C (eds). Springer International Publishing AG: Cham, Switzerland, 2017; 1–17. https://doi.org/10.1007/978-3-319-51724-7_1.
29. Corinto F, Forti M. Memristor circuits: Flux–charge analysis method. *IEEE Transactions on Circuits and Systems I: Regular Papers* 2016; **63**(11):1997–2009. https://doi.org/10.1109/TCSI.2016.2590948.
30. Ascoli A, Lanza V, Corinto F, Tetzlaff R. Synchronization conditions in simple memristor neural networks, advances in nonlinear dynamics and control. *Journal of The Franklin Institute* 2015; **352**(8):3196–3220. https://doi.org/10.1016/j.jfranklin.2015.06.003.
31. Chua LO, Yang L. Cellular neural networks: Theory. *IEEE Transaction on Circuits and Systems–I* 1988; **35**(10):1257–1272.
32. Chua LO, Yang L. Cellular neural networks: Applications. *IEEE Transaction on Circuits and Systems–I* 1988; **35**(10):1273–1290.
33. Tzouvadaki I, Jolly P, Lu X, Ingebrandt S, de Micheli G, Estrela P, Carrara S. Label-free ultrasensitive memristive aptasensor. *Nanoletters* 2016; **16**(7):4472–4476.
34. Tzouvadaki I, Aliakbarinodehi N, De Micheli G, Carrara S. Memristive effect as a novelty in drug monitoring. *Nanoscale* 2017; **9**(27):9676–9684. https://doi.org/10.1039/C7NR01297G.
35. Ibarlucea B, Akbar TF, Kim K, Rim T, Baek CK, Ascoli A, Tetzlaff R, Baraban L, Cuniberti G. Ultrasensitive detection of ebola matrix protein in a memristor mode. NanoResearch, Tsinghua University Press, 2017; (12pp). https://doi.org/10.1007/s12274-017-1720-2.
36. Kvatinsky S, Belousov D, Liman S, Satat G, Wald N, Friedman EG, Kolodny A, Weiser UC. MAGIC – Memristor aided loGIC. *IEEE Transactions on Circuits and Systems II: Express Briefs* 2014; **61**(11):1–5.
37. Ben Hur R, Wald N, Talati N, Kvatinsky S. SIMPLE MAGIC: Synthesis and in-memory maPping of logic execution for memristor-aided loGIC. *IEEE/ACM International Conference on Computer-Aided Design (ICCAD)*, Irvine, California, USA, 2017; (8pp).
38. Hild M, Siedel T, Benckendorff C, Kubisch M, Thiele C. Myon: Concepts and design of a modular humanoid robot which can be reassembled during runtime. *Proceedings of the 14th International Conference on Climbing and Walking Robots and the Support Technologies for Mobile Machines*, France, Paris, 2011.